SAND2023-07856J

Fred Gelbard[a*], Bradley A. Beeny[a], Larry L. Humphries[a], Kenneth C. Wagner[a], Lucas I. Albright[a], Max Poschmann[b], and Markus H. A. Piro[b]

[a]Sandia National Laboratories, 1515 Eubank S. E., Albuquerque, New Mexico 87123

[b]Ontario Tech University, Oshawa, ON, Canada

*E-mail: fgelbar@sandia.gov

57 Pages

14 Figures

No Tables

Application of MELCOR for Simulating Molten Salt Reactor Accident Source Terms

Abstract - *Molten salt reactor systems can be divided into two basic categories: liquid-fueled Molten Salt Reactors (MSRs) in which the fuel is dissolved in the salt, and solid-fueled systems such as the Fluoride-salt-cooled High-temperature Reactor (FHR). The molten salt provides an impediment to fission product release as actinides and many fission products are soluble in molten salt. Nonetheless, under accident conditions, some radionuclides may escape the salt by vaporization and aerosol formation, which may lead to release into the environment. We present recent enhancements to MELCOR to represent the transport of radionuclides in the salt and releases from the salt. Some soluble but volatile radionuclides may vaporize and subsequently condense to aerosol. Insoluble fission products can deposit on structures. Thermochimica, an open-source Gibbs Energy Minimization (GEM) code, has been integrated into MELCOR. With the appropriate thermochemical database, Thermochimica provides the solubility and vapor pressure of species as a function of temperature, pressure, and composition, which are needed to characterize the vaporization rate and the state of the salt with fission products. Since thermochemical databases are still under active development for molten salt systems, thermodynamic data for fission product solubility and vapor pressure may be user-specified. This enables preliminary assessments of fission product transport in molten salt systems. In this paper, we discuss modeling of soluble and insoluble fission product releases in a MSR with Thermochimica incorporated into MELCOR. Separate effects experiments performed as part of the MSRE (Molten Salt Reactor Experiment) in*

which radioactive aerosol was released are discussed as needed for determining the source term.

Keywords - Molten salt, fission product release, non-LWR MELCOR, MSR, FHR.

Note – *Some figures may be in color only in the electronic version.*

I. INTRODUCTION

"MELCOR is a fully integrated, engineering-level computer code whose primary purpose is to model the progression of accidents in light water reactor nuclear power plants. A broad spectrum of severe accident phenomena in both boiling and pressurized water reactors is treated in MELCOR in a unified framework. Current uses of MELCOR include estimation of fission product source terms and their sensitivities and uncertainties in a variety of applications."[1] Currently, MELCOR is being enhanced to also model non-LWR (non-Light Water Reactor) accidents by adding non-LWR submodels. In this work we present the Generalized Radionuclide Transport and Retention (GRTR) submodel within MELCOR. The GRTR can model molten salt behavior over a timestep in a MELCOR control volume. MELCOR still controls the flow of mass and energy among many control volumes over time for a simulated accident. The details of MELCOR are given elsewhere[1,2] and will not be repeated in this work. Instead, this work concentrates on the GRTR molten salt submodel that is now contained within MELCOR.

Molten salts have been proposed as a coolant because they have a broad temperature range over which they are liquid and therefore do not require high pressures to operate, have a high thermal conductivity, and are chemically stable.[3] For liquid-fueled MSRs, fuel and some fission products are soluble in the salts.[4,5] Thus, a chemical processing unit outside of the reactor could be used to remove the fission products in situ, and then return the processed salt for further heat

production without requiring reactor shutdown. However, insoluble fission products could deposit on structural surfaces such as heat exchangers, which would reduce heat transfer and concentrate radionuclides on such surfaces. Removing deposited fission products may require the reactor to shut down. Therefore, controlling the salt chemistry so that soluble fission products are formed is preferred. For solid-fueled MSRs, the fuel and fission products are isolated from the coolant, e.g., TRISO (TRi-structural ISOtropic) particles within pebble fuel elements. Thus, for these reactors, the radionuclides are isolated from the salt during normal operations. However, a severe accident may result in the rupture of TRISO particles in a compact, which could release radionuclides into the salt coolant.

For both solid-fueled and liquid-fueled MSRs, a very attractive feature of molten salts is that the salt provides an impediment to radiological releases in the event of an accident. The GRTR submodel added to MELCOR can be applied to molten salt coolants in which radionuclides are released into or are already present in the salt, respectively.

The fission products have been classified into three forms: salt-seeking elements, noble-metal elements, and noble gases.[3,6] Salt-seeking elements are generally soluble in the salt, whereas noble elements are not. A graphical display of the solubility state in salt of some elements in the periodic table is available.[7] In this format, a fourth form was added of "sometimes soluble" elements. Other workers have made a similar characterization of the fission products for the MSRE (Molten Salt Reactor Experiment) at ORNL (Oak Ridge National Laboratory).[5,8] More recently, three forms have been used to indicate solubility.[9]

I.A. Conceptual Framework of MELCOR Molten Salt Reactor Severe Accident Model

The GRTR framework builds on the ideas of classifying radionuclides into different forms and allows for a user-specified number of forms and mass transfer between forms. For molten salt applications, GRTR is configured to quantitatively track the masses of all species in a salt pool in five forms depending on both the solubility state and location of species in an MSR. This refined level of detail is necessary to capture the states and locations of radionuclides as observed in the MSRE.[8] However, the model does not require that a species be entirely soluble or insoluble, or in a single form. Therefore, a species can exist in more than one form and at different concentrations in each form. The amount of a species in each form is calculated by the GRTR submodel as a function of time, temperature, pressure, and salt composition.

A schematic of the GRTR submodel for molten salts is given in Fig. 1. Shown in the top row of Fig. 1 are the five forms of the radionuclides. The inputs to the GRTR submodel include the control volume temperature, the control volume pressure, and the masses of all components in the five forms at the beginning of a timestep. Form 1 in the top-left corner of the first row is for soluble or salt-seeking radionuclides. If a component has reached its solubility limit, the insoluble mass in the salt may remain suspended in the salt, migrate to the top of the salt pool, or deposit on to fixed structural surfaces in contact with the salt. These three forms are shown in Fig. 1 as Forms 2, 3, and 4, respectively. Horizontal arrows indicate mass transfer processes, with dashed and undashed lines to distinguish among these processes. Form 5 is for gases such as Kr, Xe, and possibly tritium or tritium fluoride, given as NCG (Non-Condensible Gases) in Fig. 1. For the next step, as given in the second row, the GRTR submodel performs an equilibrium calculation. At the user's option, Thermochimica may be used to determine the equilibrium masses of soluble and insoluble species, and the vapor pressure of volatile species. This calculation is performed for all phases and all states simultaneously, and not for each phase

or state separately. If there are insufficient data for Thermochimica, the user may instead provide a function input for fission product solubilities and vapor pressures. Such functions can be provided in the MELCOR input stream. The GRTR submodel then relocates the masses in Forms 1, 2, and 5 according to the equilibrium results. Only the forms pointed to by an arrowhead indicate mass transfer, with the form covered by the dashed part not to be included.

The next GRTR submodel calculation step, which is shown in the third and fourth rows in Fig. 1, is to determine the transport among the five forms, and releases to the cell atmosphere, respectively. In this step, there are three transport processes within the forms. Insoluble fission products may transport between the interface layer and the pool. The second process is transport from suspended insoluble fission products to deposit on heat structures in contact with the salt. The third process is transport of insoluble material between the pool and deposits on surfaces in the core. Aerosols may be formed from the condensation or nucleation of volatile species that are released to the gas space. However, since this process occurs in the atmosphere above the pool, it is therefore modeled with MELCOR's existing radionuclide vapor and aerosol model. The state of the pool, deposited mass on surfaces, and the released masses are passed back to MELCOR for transport within a facility. The equations describing the transport between forms and to the atmosphere above the pool are given later in this work. The three gas space releases given in highlighted boxes in the bottom row are (1) volatile vapor, (2) aerosol particles from the interface layer at the top of the salt pool, and (3) gases such as Xe and Kr. The direct release of aerosol from the top of the salt pool to the vapor space is discussed later in much detail.

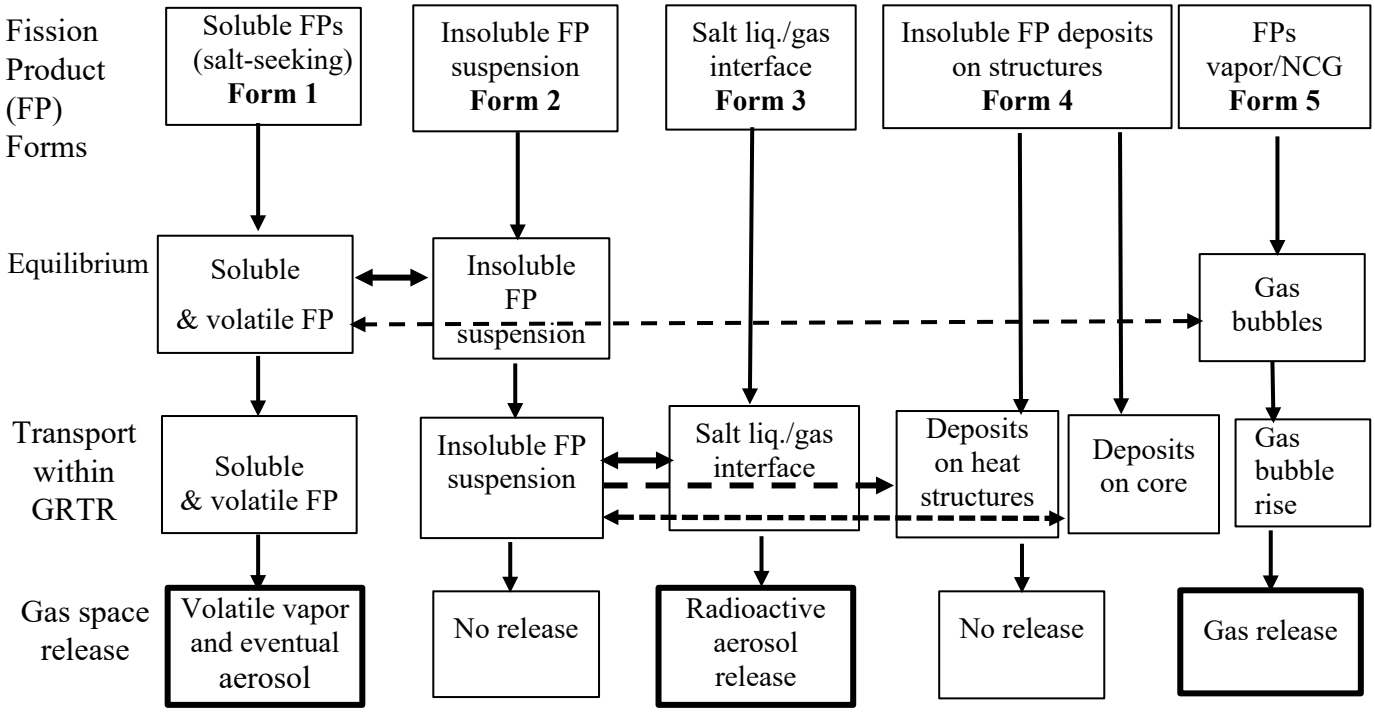

Fig. 1. Schematic of the analysis steps of GRTR (Generalized Radionuclide Transport and Retention) submodel in MELCOR. The calculations performed are equilibrium, and then simultaneous transport occurs within the pool and to the gas space.

I.B. GRTR (Generalized Radionuclide Transport and Retention) Model Data Requirements

To model the transport and release of radionuclides in the five forms, the three categories of properties needed are: (1) thermophysical, (2) thermochemical, and (3) mass transfer properties of the salt and the fission products. Thermophysical properties such as density, heat capacity,

thermal conductivity, melting point, boiling point, viscosity and surface tension have been compiled for pure salts.[10-14]

Thermochemical properties such as fission product solubility and vapor pressure as a function of temperature and salt composition have not been as extensively reported but some data are available. Thermochimica[15,16,17] is now included in MELCOR to determine fission product solubility and vapor pressure. The (optional) use of Thermochimica to calculate solubility and vapor pressure requires that a suitable thermodynamic database be supplied by the user. Thermochimica is compatible only with databases in the ChemSage DAT format. Ultimately it is at the user's judgement to determine what constitutes a suitable database, but in general the database should contain data for all elements of interest and represent all known or important phases of chemical system. Whenever possible, experimental corroboration of the database should be sought for outputs crucial to accident analyses (for example, vapor pressures).

The JRCMSD (Joint Research Centre – Molten Salt Database) 2021 version was used in this work.[18,19,20] This database uses the modified quasichemical model in the quadruplet approximation (MQMQA)[21,22] to represent the molten salt phase. Thermochimica is compatible with MQMQA[23] and calculates the equilibrium vapor pressures and solubility for the temperature, pressure, and composition conditions determined by MELCOR.

No transport property data has been found in the literature for the third category, such as diffusivity of the fuel and fission products in the salt and in the gas phase at high temperatures. Properties in this category are estimated using correlations.[24]

Accident analyses require these three property categories for pure salts with fission products and also for the effects on these properties from contaminants, such as water vapor, oxygen,

abraded graphite particles, and corrosion products. Since severe accidents can extend to high temperatures significantly above normal operating temperatures, a wide temperature range is also needed. Obtaining all the property data given above for an accurate radionuclide release model due to a severe accident is a daunting task. However, a system level code such as MELCOR is a viable tool for assessing sensitivities, uncertainties, and ranking the importance of different properties on radionuclide releases. Thus, an important application of the GRTR submodel in MELCOR is for determining parameter sensitivities to help prioritize research efforts.

I.C. Paper Organization

Section II discusses the results of the thermochemical property literature survey. Much has been learned from the work at ORNL with the MSRE.[4,5,8] Some general statements in the literature on fission product solubility have been reported. Data on the solubility limits for He, Kr, Xe, PuF_3, AmF_3, CeF_3 are available. For quantitative analysis that can be applied to a wide range of salt compositions and temperatures, species solubility limits and vapor pressures may be determined by the Thermochimica code[15-17] at the users' discretion if the appropriate database is available.

Predictions of solubility and vapor pressure by Thermochimica are compared to data. By using equilibrium thermodynamics, we implicitly assume that the timescale for reactions to reach equilibrium is much shorter than the timescale for the accident events. Furthermore, the transport of reactants and products is assumed not to be limiting within the control volume, and thus the fluids are well-mixed. A similar approach using MELCOR but with a different GEM code external to MELCOR was reported recently for determining vaporization of fission

products Cs and I from a fluoride salt.[25] MELCOR provides the distributions of radionuclides within a facility and the source term from a facility for a hypothetical severe accident. This information may be used by other codes such as MACCS[26] to determine atmospheric transport, deposition, and consequences of ground and cloud shine. Discussions of MACCS are beyond the scope of this work.

Section III presents a discussion of research related to radioactive aerosol release. Experiments performed with a small sample of radioactive MSRE salt showed that very small particles, less than 10 micrometers in diameter, are released even under quiescent conditions at a temperature of 600 °C. Another release mechanism is bubble bursting, which has been shown to release particles from aqueous solutions and may also do so in molten salt. As bubbles reach the liquid pool/gas interface, the bursting of the liquid film at the pool gas interface provides a mechanism for particles of soluble species to be released directly into the gas space. Chemically inert gas bubbles may be directly introduced into the salt to purge radioactive gases. In the MSRE, helium was used as the purge gas. Bubbles may also form during an accident by agitation of the salt due to splashing and sloshing, which engulfs gas. Using CFD (Computational Fluid Dynamics), we explore possible experimental artifacts that may inadvertently cause salt to contaminate surfaces that are analyzed to determine radionuclide releases from the salt.

Section IV discusses the integration of the GRTR submodel into MELCOR. As mentioned previously, there are five possible forms where radionuclides can exist in a molten salt pool, and MELCOR tracks the radionuclide masses in all these forms. For each control volume in a MELCOR model which has salt in the control volume, the GRTR submodel allows for transport among these five forms. Radionuclides in Forms 1, 3, and 5 can lead to vapor or aerosol releases

to the environment. In addition, radionuclides may deposit on surfaces in contact with the salt, and this may complicate operations. Once a radionuclide is transported out of the molten salt either by vaporization, aerosolization, or deposition on to surfaces, the existing MELCOR models are used to track these species within the reactor and containment.

Section V discusses an application of MELCOR with the vaporization of cesium from a FLiBe salt for a proposed MSR power plant. Finally, Section VI presents a summary of the current capabilities and suggests some needed experiments.

II. RADIONUCLIDE SOLUBILITY AND VAPOR PRESSURE DATA IN MOLTEN SALT

II.A. Radionuclide Solubility

From a safety perspective, soluble fission products are not easily released as either vapor or aerosol. To maximize fission product solubility, an oxidizing solution is desirable in which the fission product atoms lose electrons by forming fission product fluorides or chlorides. However, there are structural metals such as steel and Hastelloy used for piping and vessels for which oxidation (which would be corrosion to form a fluoride or chloride), is very undesirable. For these metals, a reducing salt solution is desirable. Thus, the ideal molten salt is oxidizing for fission products but reducing for structural metals. This balance was achieved in the MSRE at ORNL by controlling the UF_4/UF_3 molar ratio at ~100. This ratio increased as uranium fissioned and thereby releasing fluorine into the salt, which formed UF_4. Beryllium was introduced and reacted with the UF_4 to form UF_3 and BeF_2. Essentially, the beryllium may be viewed as a

sacrificial metal to maintain a desired buffering effect. With this reaction, corrosion in the MSRE was minimal at ~2.5×10^{-3} mm/yr (0.1 mil/yr), but there were still insoluble fission products.[5]

Solubility is dependent on the redox potential of the salt and temperature.[4,6,27,28] Solubility data of Pu, Ce, and Am in fluoride salts has been reported.[29-34] An example of PuF_3 solubility as a function of temperature and composition is given in Fig. 2 as dots for the data,[29] and as a solid curve predicted with Thermochimica using the JRCMSD.[18] The log of the solubility varies essentially linearly with the inverse absolute temperature, thereby showing Arrhenius-like behavior. As can be seen from Fig. 2, the agreement between the Thermochimica predictions with the JRCMSD and the experimental data is good. PuF_3 is soluble in FLiBe and PuF_3 solubility increases with increasing temperature. However, there is a solubility limit for a given temperature and salt composition. This limit is first checked in the GRTR submodel to determine whether new insoluble material is added as suspended particles or existing suspended material is dissolved.

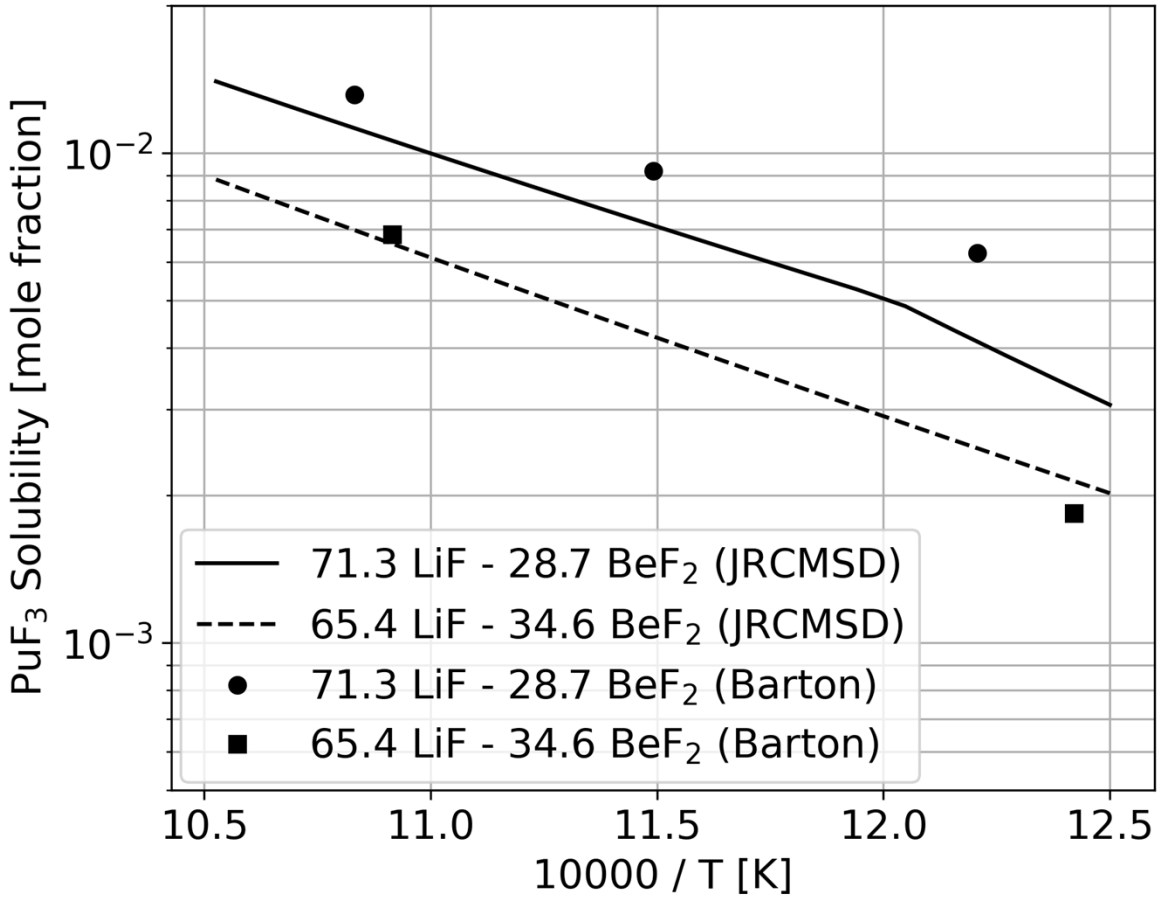

Fig. 2. Solubility of PuF_3 in FLiBe at the mole percentage given in the legend for the data[29] and calculated with Thermochimica using the JRCMSD.[18]

For solid-fueled reactors in which the fuel and fission products are generally isolated from the salt under normal operating conditions, fission product solubility may not be as important during normal operations. For TRISO fuel at high temperatures, Ag-110m has been shown to migrate through intact TRISO particles[35] and should be insoluble in fluoride salts.

There are also data for cesium and iodine fission products in molten salt.[20,36] In the GRTR submodel, users may either specify a solubility limit or invoke Thermochimica to determine solubility limits with the JRCMSD.[18] Other databases may be utilized by MELCOR/GRTR in a

separate file at the users' discretion. For soluble fission products that are volatile, the GRTR will pass the vaporized mass over a timestep to MELCOR. Upon encountering a cooler atmosphere, the volatile species may nucleate and form aerosol particles.

II.B. Insoluble Fission Product Form

If the fission product is not soluble and is not a vapor, then such atoms may be isolated. The atoms may form atomic clusters or attach to existing particles in the molten salt to form a suspension. A suspension of small particles that are 1-1000 nm in diameter in a liquid is called a colloid.[37] The GRTR submodel tracks insoluble particles using Forms 2, 3, and 4, which are, respectively, insoluble suspension, insoluble particles at the interface between the molten salt pool and the gas space, and deposited particles on fixed surfaces. The dynamics of these three forms shown in Fig. 1 are discussed in Section IV of this work.

II.C. Vapor Pressure in Molten Salt

An attractive feature of molten salt with soluble fission products is that solution effects can greatly impede vaporization of such fission products. Consider cesium, which has a normal boiling point of 944 K, and therefore a vapor pressure of 101 kPa at this temperature. However, if small amounts of cesium are in FLiBe, as given in Fig. 3, the cesium vapor pressure is less than 1.5×10^{-4} Pa at 944 K. That is a reduction by a factor of about 7×10^{8} in vapor pressure, which greatly reduces the rate at which cesium would vaporize. Nonetheless, we term the solubility effect on vaporization as an impediment to release to the atmosphere and not an absolute barrier. As will be shown later, even this very small vapor pressure over time and at high temperatures can still vaporize a noticeable amount of cesium in FLiBe. Insoluble fission products are obviously not impeded from vaporizing by the solubility effect, but the salt can provide some impedance of transport to the atmosphere even for insoluble fission products.

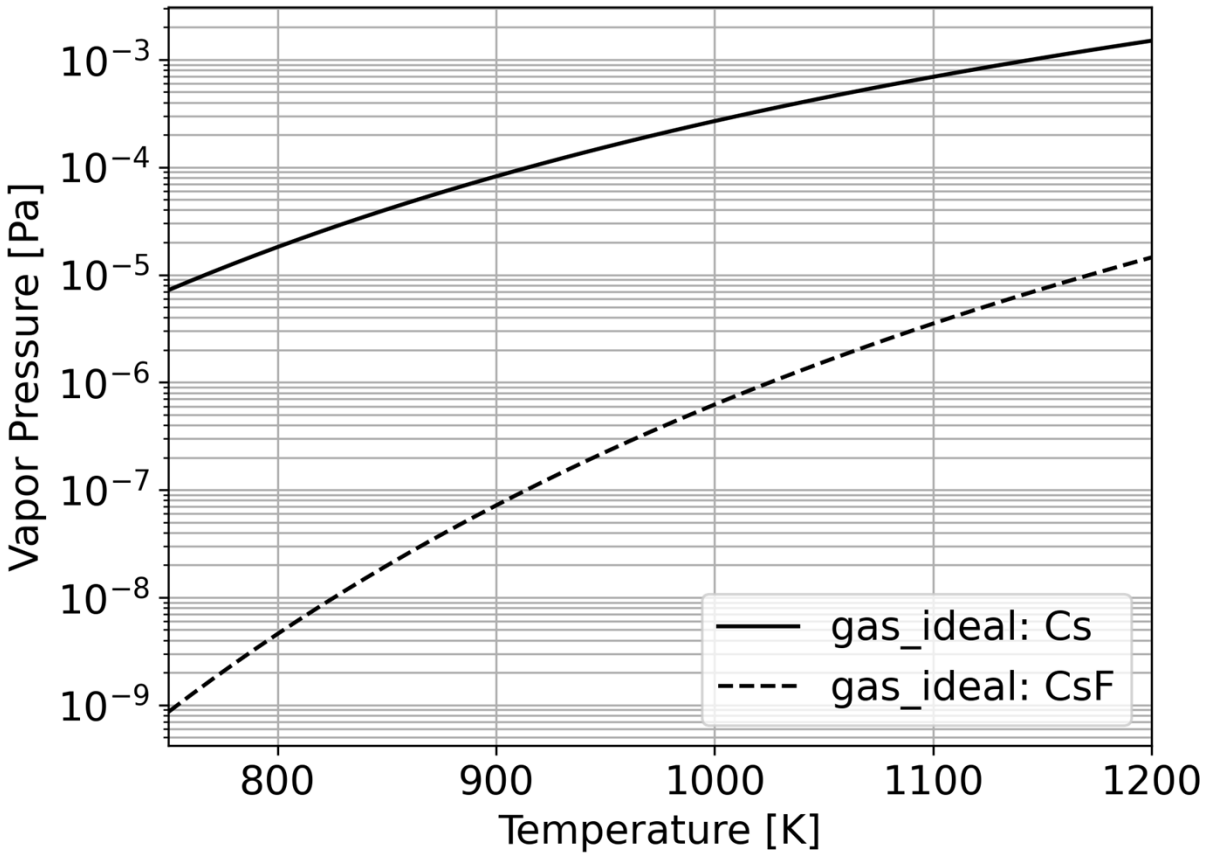

Fig. 3. Predicted vapor pressure of cesium and cesium fluoride over molten FLiBe using Thermochimica. 2.384 g of Cs were dissolved in 42 m^3 of FLiBe. The JRCMSD was used as the thermodynamic database.

To further assess the accuracy of Thermochimica/JRCMSD vapor pressure predictions, these predictions are compared to data in Fig. 4. For a salt with 90 mol Li, 10 mol Be, 0.09 mol Rb, and 110.09 mol F, the predicted vapor pressures are given as curves, and the experimental data[38] are given as points. While the calculated vapor pressures systematically underestimate the experimental measurements, they are correct within an order of magnitude and reproduce the correct temperature trend and ordering.

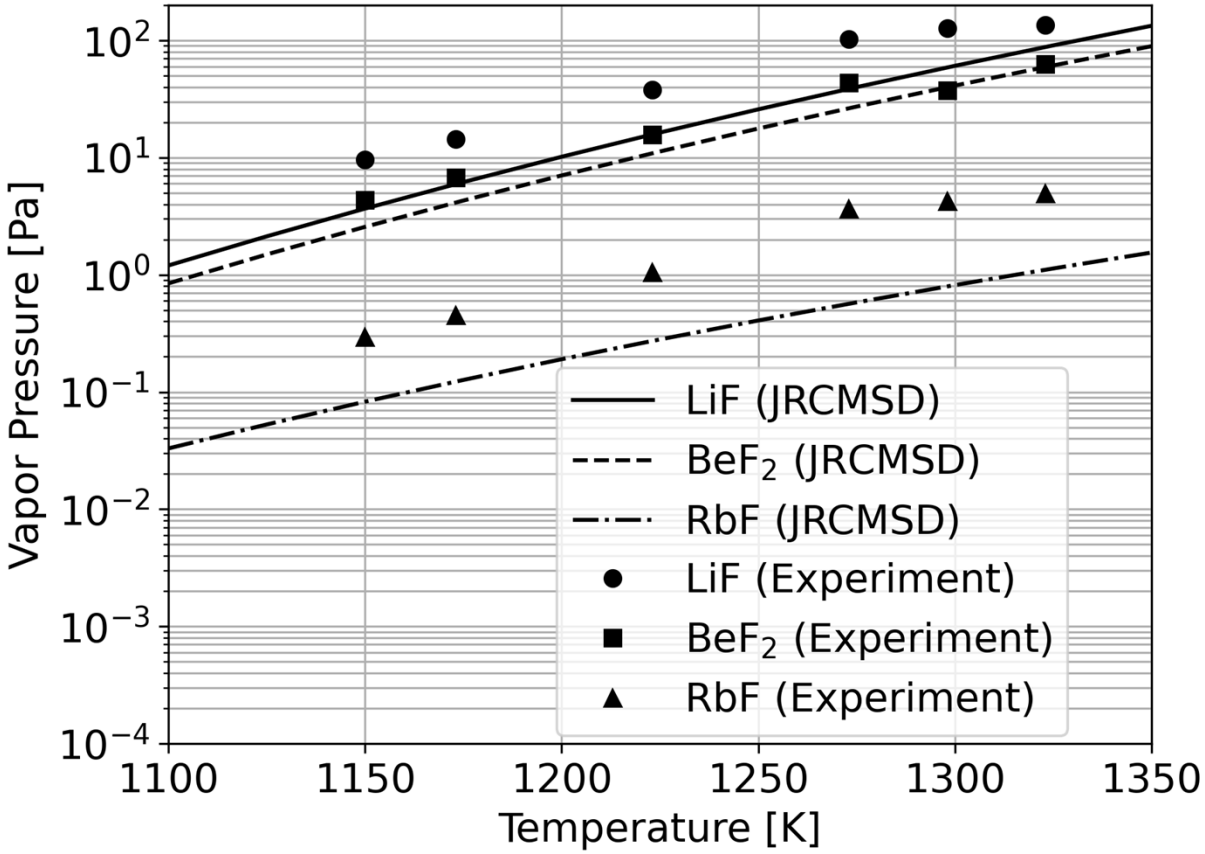

Fig. 4. Vapor pressures of LiF, BeF_2, and RbF over a molten salt using Thermochimica and JRCMSD compared to experimental data.[38]

III. RADIONUCLIDE AEROSOL RELEASE

III.A. Aerosol Releases During Operation of the MSRE

Whether the fission products are insoluble or soluble, the liquid salt provides an impediment to release. However, a severe accident may involve considerable splashing and agitation of the

salt. A liquid film or jet may be expelled by these processes with the film or jet breaking up to form droplets. These droplets are generally larger than 100 micrometers in diameter and may be a local contamination problem but are not considered respirable. Respirable particles are most often defined as particles with an aerodynamic diameter of 10 micrometers or less.[39] Such small particles are readily transported, and if inhaled, may deposit in the lungs creating a health hazard.

Agitation may also entrain gas and thereby form bubbles in the molten salt. Bubble bursting releases two types of liquid droplets in aqueous solutions.[40,41] Similar phenomena may also occur with molten salt but that has yet to be proven. When the depression in the liquid due to the bubble is filled in by the surrounding liquid, for aqueous solutions an upward liquid jet forms that disintegrates into droplets that are generally not respirable. However, the cap of the bubble is a thin liquid film that may be on the order of a micrometer thick or less.[42,43] When the cap ruptures, respirable droplets may form of a size comparable to the liquid film thickness. Consequently, if the same phenomena occur in molten salt, soluble fission products and insoluble particles that are in the film may be aerosolized.[44]

For the MSRE, molten salt aerosolization was reported as mist due to agitation and bubbles.[45,46] "The origin of most of the mist in the MSRE pump bowl is undoubtedly the spattering and splashing of the streams from the spray ring."[46] The same report later states, "the pump bowl difficulties were caused by an aerosol-type dispersion of salt particles."[46] The basis for describing the particles as aerosol-type is unclear since no particle size distribution is given. Fig. 5 below (which is Fig. 4 in reference [46]), shows spherical droplets collected from the gas space above the salt. Using the 1/2-inch width of the strip for scaling, the smallest particle is estimated to be 100 micrometers in diameter with most of the particles being much larger. Such particle sizes are generally not considered to be aerosol particles. The particles in Fig. 5 may be

due to the breakup of the liquid jet or crown from splashing. In addition, because the sample shown is time-integrated over 12 hours, possibly smaller droplets were deposited that coalesced over time into much larger droplets as shown in Fig. 5. The report later states that "A filter about 15 ft downstream from the pump bowl trapped salt particles (all 10μ or smaller) at a rate of about a cubic inch per 100 hours of salt circulation."[46] If the parenthetical remark, "all 10μ or smaller" as given in the report corresponds to 10 micrometers diameter or smaller, then this would be very good evidence of respirable aerosol release in normal operating tests for the MSRE.

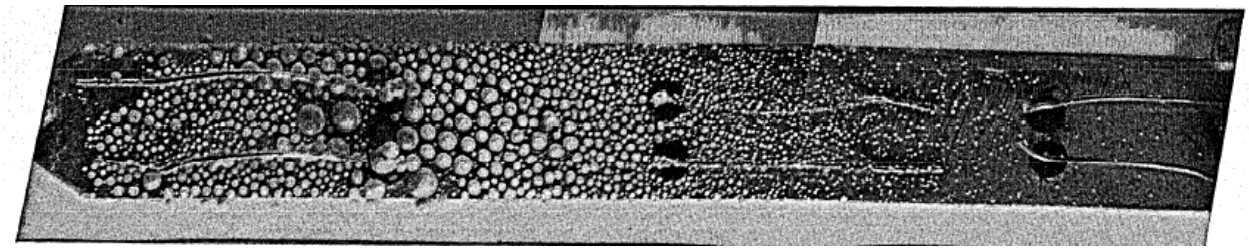

Fig. 5. Photograph of droplets on a ½ inch (12.7 mm) wide metal strip exposed in the MSRE pump.[46]

From the statements and observations in reference [46] as given above, salt agitation by splattering and splashing is the mechanism for the release of aerosol-type particles. Agitation can be expected in a severe accident and therefore a quantitative model is needed of the amount and size of droplets produced by agitation. Fortunately, carefully controlled separate-effects experiments were conducted to assess the effects of bubbling and sweeping gas flow across the surface of irradiated molten salt on aerosol production.[47] As we discuss next, these experiments show that there may be other or more important mechanisms for respirable fission product aerosol releases.

III.B. Aerosol Releases in Separate Effects Experiments

The mechanisms for the observed respirable aerosol formation were explored in separate effects experiments as part of the MSRE.[47,48] A schematic of the apparatus from reference [47] is given in Fig. 6. Two types of flow experiments were performed, either gas sweeping-flow experiments as diagrammed in Fig. 6 in which the gas was introduced significantly above the salt surface, or gas bubbling-flow experiments in which the inlet tube extended 3.5 inches (88.9 mm) below the salt surface. These two types of flow experiments are shown schematically on the left and right sides of Fig. 7, respectively. The opening to the nickel outlet tube (called the probe tube) was positioned ¼-inch (6.35 mm) above the salt surface.[47] However, in a subsequent report[48, p. 145] the probe tube inlet is given as being between ¼ and ½ inches (6.35 and 12.7 mm, respectively) above the salt surface. As discussed later, this slight modification of the gap distance between the salt and the opening of the outlet tube may be important. A 50 gram sample of MSRE salt was maintained at 600 °C inside the gas-tight stainless steel reaction vessel that was inside a tube furnace that was inside a hot-cell. Gas consisting of either pure helium or helium with 5% hydrogen was introduced through the inlet tube at 10-15 cm^3/minute.[47,48] The dimensions given in Fig. 7 are estimated from scaling the dimensions given in Fig. 6 with the constraints that the reaction vessel was cylindrical, the gap was ¼-inch (6.35 mm), the depth had to be enough to accommodate a 3.5 inch (88.9 mm) long tube beneath the salt surface, and the volume of the salt was 22.1 cm^3 based on a mass of 50 grams and a density of 2.267 g/cm^3 at 600 °C [reference 8, Table 2.1]. Estimated values have an asterisk preceding the numerical value in

Fig. 7. These values are used in the CFD (Computational Fluid Dynamics) simulation to be discussed later.

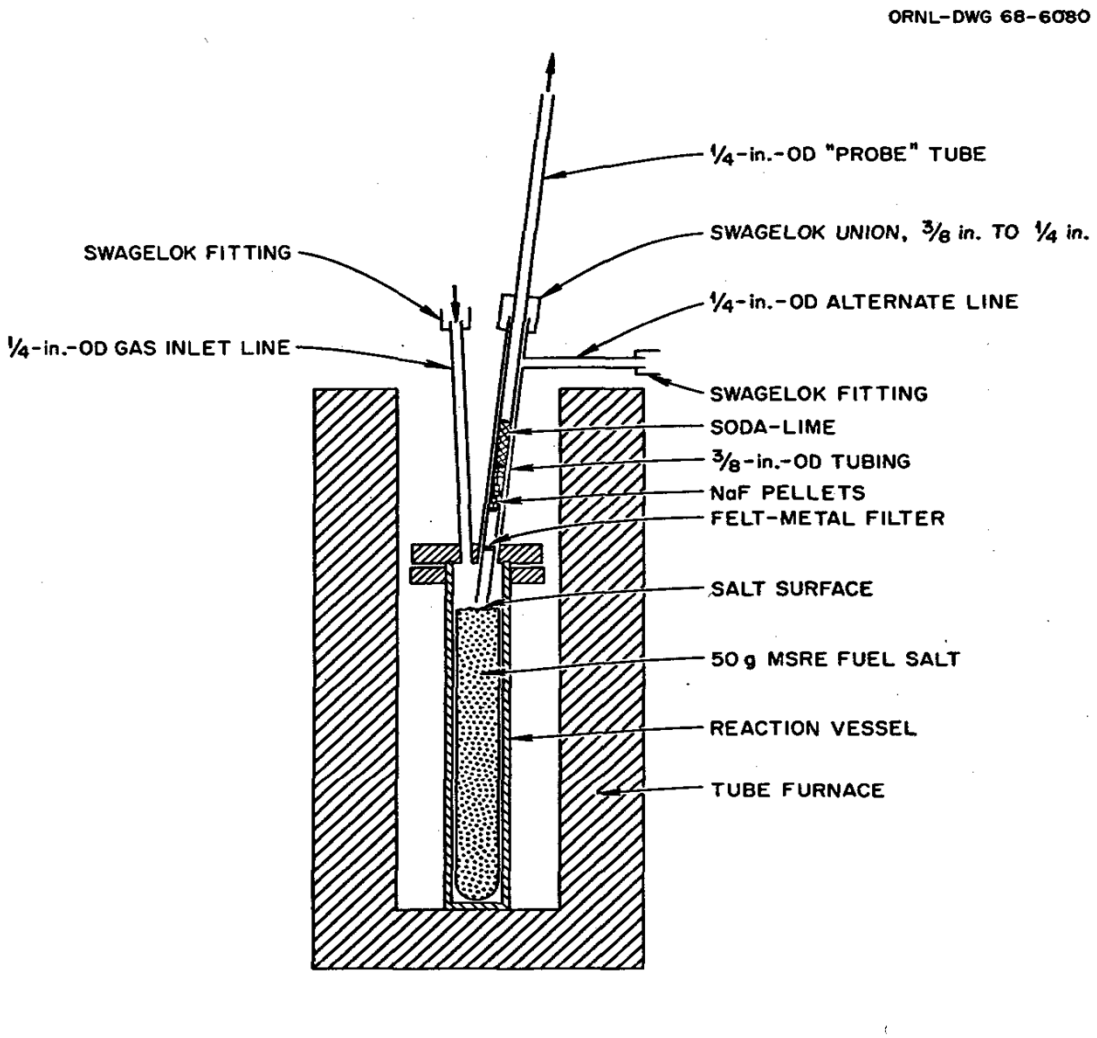

Fig. 10.2. Hot-Cell Test Reaction Vessel.

Fig. 6. Schematic drawing from reference [47] for gas sweeping-flow experiments.

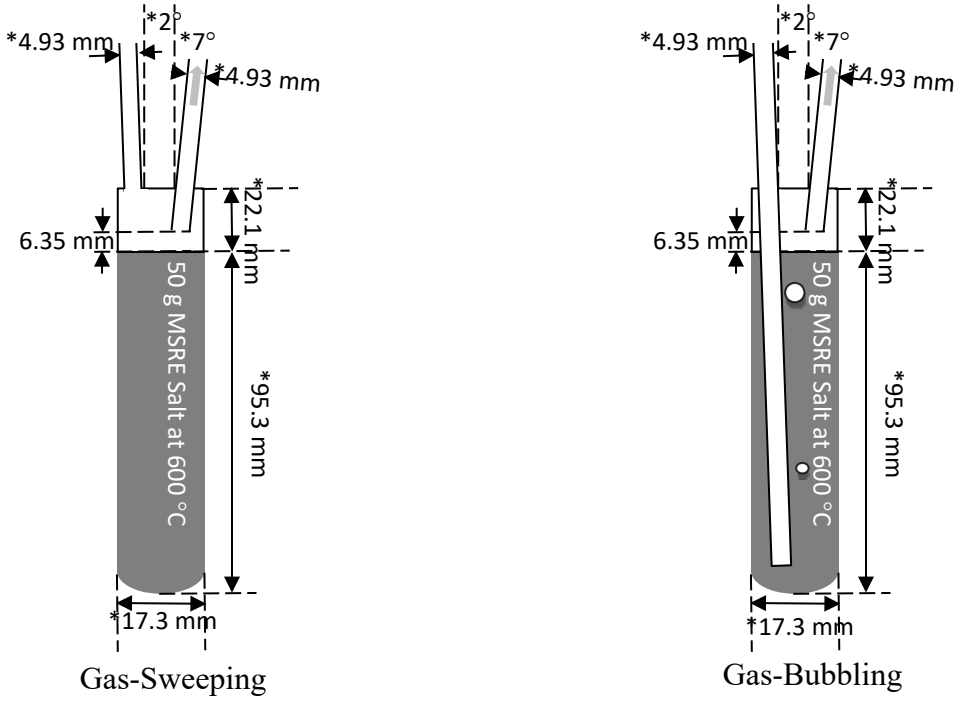

Fig. 7. Dimensions of our computational model for gas-sweeping and gas-bubbling flow on the left and right side, respectively. Numerical values that are estimated are preceded with an asterisk. The diameters of the tubes and reaction vessel are the estimated inner diameters.

After a flow experiment, the probe tube was cut into four sections described as: (1) bottom inch of the probe tube, (2) felt-metal, (3) NaF pellets, and (4) soda-lime. The last three regions are labelled in Fig. 6. The felt-metal filter was 1/16-inch (1.6 mm) thick and is described as having "100% retention of particles larger than 4 μ".[47] This implies that particles deposited in the NaF-pellet and soda-lime regions are no larger than 4 micrometers in diameter. Gamma ray spectroscopy was used to identify radionuclides and determine activities in each of the four sections after the exterior of the tube was cleaned to remove contamination.

In one series of sweeping-flow tests,[47] six 1/8 inch diameter copper screens of the type used to hold electron microscope specimens were spaced at 12.7, 25.4, 38.1, 63.5, 88.9, and 114.3 mm (½, 1, 1.5, 2.5, 3.5 and 4.5 inches, respectively) from the molten salt surface. The gas exiting the reactor passed at a linear velocity of about 0.5 cm/sec for 40 minutes. The screens at 63.5, 88.9 and 114.3 mm (2.5, 3.5 and 4.5 inches, respectively) above the molten salt contained three sizes of particles collected from the gas phase above a 50 gram salt sample as shown in Fig. 6. The smallest particles had diameters of 3.5-18 nm, the medium size had diameters of 100-200 nm, and there were particles that were described as more than ten times the medium diameter size. In a subsequent report in reference [48, p. 145], the largest particles are described as several micrometers in diameter. Such particles are all respirable and therefore of concern. An electron micrograph that provided data for these small aerosol particles is shown below in Fig. 8. When this collection technique was later tried four times again, aerosol particles were not collected as stated in reference [48, p. 148]. The problem was attributed to sample handling difficulties.

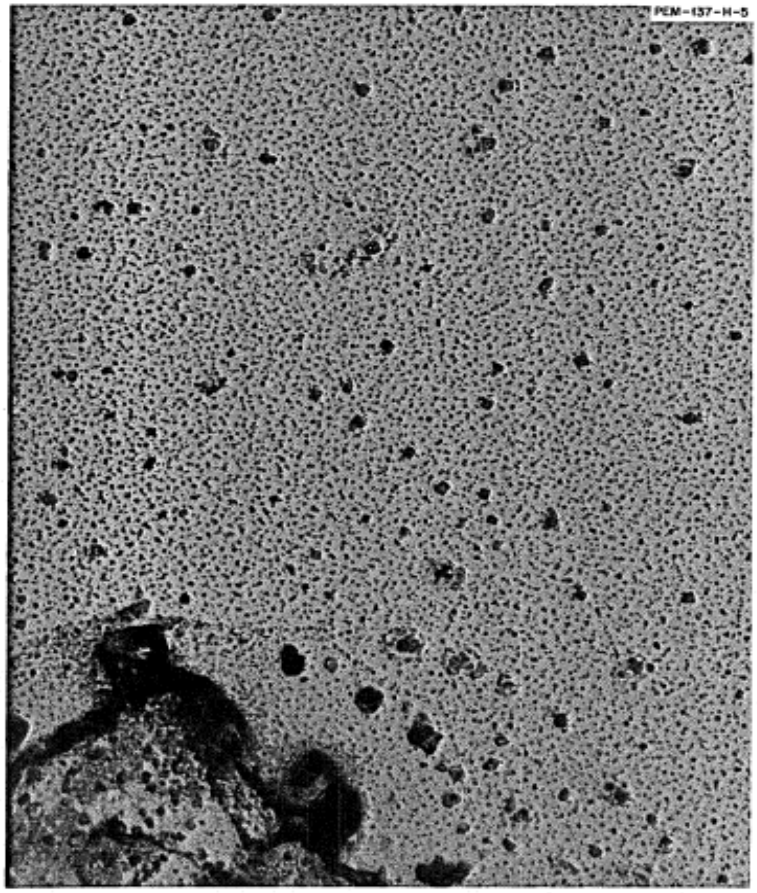

Fig. 10.4. Electron Micrograph of Particles in Gas Flowing over MSRE Salt. 88,000x.

Fig. 8. Electron microscope image of particles collected from the gaseous headspace above a 50-gram molten salt sample.[47] The image has a magnification of 88,000X.

Data for pure helium and helium with 5% hydrogen given in reference [47, Table 10.4] are combined, and plotted in Fig. 9. Triangles are used for the bubbling-flow tests, and circles are used for the sweeping-flow tests. The same color is used for the same isotope for both flow types. The data in Fig. 9 were collected on 35-day old MSRE salt. In this dataset, bubbling flow produced significantly more aerosol than sweeping flow, sometimes by orders of magnitude, for all radionuclides at all four regions. The only exception is the bottom one inch

(25.4 mm) of the probe tube for Nb-95 when the activity for sweeping flow was larger than the activity for bubbling flow. These data indicate that slow bubbling at 10-15 cc/min significantly increases the aerosolized mass. "However, when the gases were bubbled rapidly through the melt for 2 min at about 200 cc/min (first test), the amounts of all activities in all sections of the probes increased by factors of 10 to 1000 compared with the slow-flow cases. Therefore the amount of fume or mist formation is greatly enhanced by turbulent gas-fuel contacting."[47, p.104] The sweeping-flow results indicate that even with just mild flow over stagnant radioactive molten salt, radioactive material is released from the salt. The sweeping-flow releases indicate that splashing and bubble bursting may not be the only mechanism for aerosol release.

As discussed in more detail,[47,48] experimental improvements were made and a larger dataset using one-day old MSRE salt given in reference [47, Table 10.5] was generated. These data are plotted in Fig. 10 and now include isotopes with shorter half-lives that could not be as reliably measured previously with 35-day old MSRE salt. The short-lived isotopes that were difficult to measure and are not included in Fig. 9 are Mo-99, Te-132 and Te-129, which have half-lives of 66 hours, 69.6 minutes and 3.2 days, respectively. From Fig. 10 we see that sweeping flow can release comparable or more radionuclide than slow bubbling flow. (The I-131 activity in the felt-metal and NaF regions was above 10^9 DPM (Disintegrations Per Minute) and is not shown in Figs. 10a and 10b.) As noted in reference [47, p. 104], "The readiness with which gaseous suspensions of noble metals and of fuel salt are formed above the highly radioactive fuel melt invalidated the original presumption that only fission products with volatile fluorides could leave the melt under the gentle sweep conditions. However, the evidence from the hydrogen gentle sweep runs and particularly from the hydrogen bubbling run in the second test is nearly incontrovertible that volatile fluorides are not involved in a significant way in causing the noble-

metal fission products to become gas borne." This has important implications that even quiescent radioactive salts at an operating temperature of 600 °C, inherently release radioactive respirable aerosol particles without agitation. We add that the particles are respirable since significant activity was detected downstream of the felt-metal filter with a cutoff diameter of 4 micrometers.

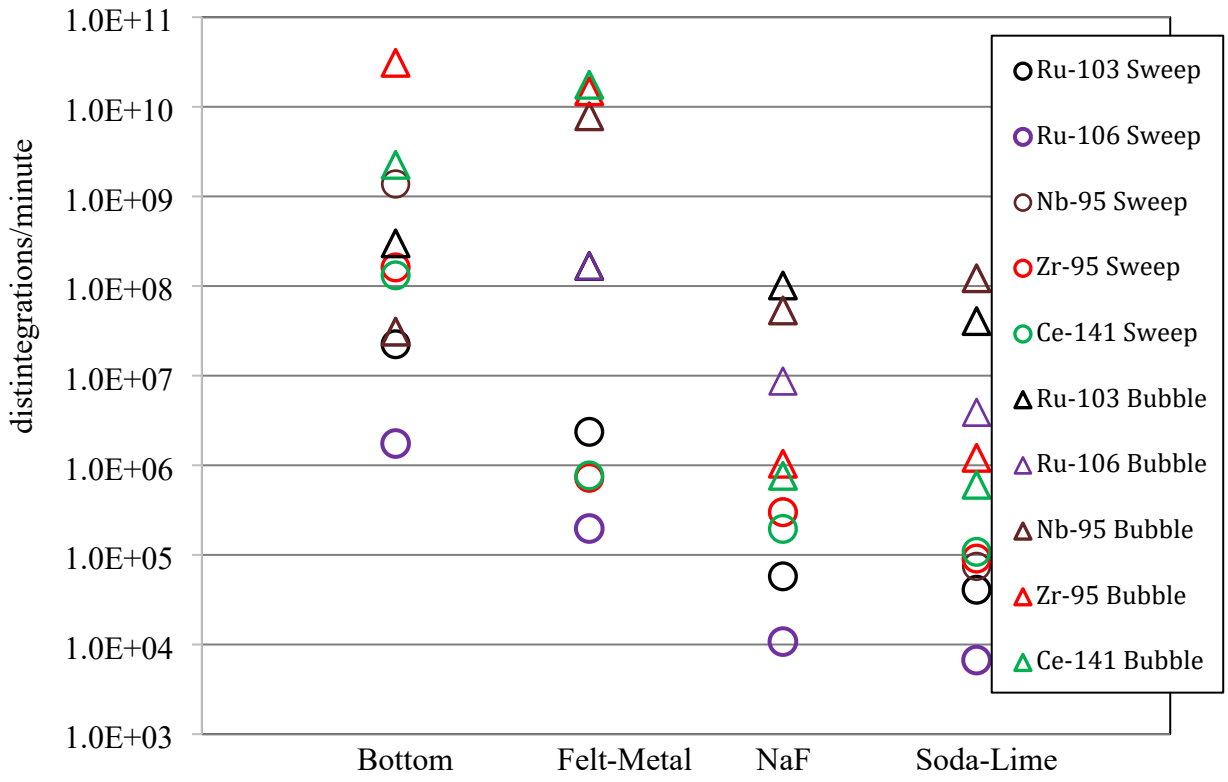

Fig. 9. Plot of average tabulated data from reference [47, Table 10.4] of activity deposited in four sections of the probe tube comparing bubbling-flow and sweeping-flow. For this dataset, the bubbled-flow tests (given by triangles) generally had significantly more radioactivity deposited than the sweeping-flow tests (given by circles).

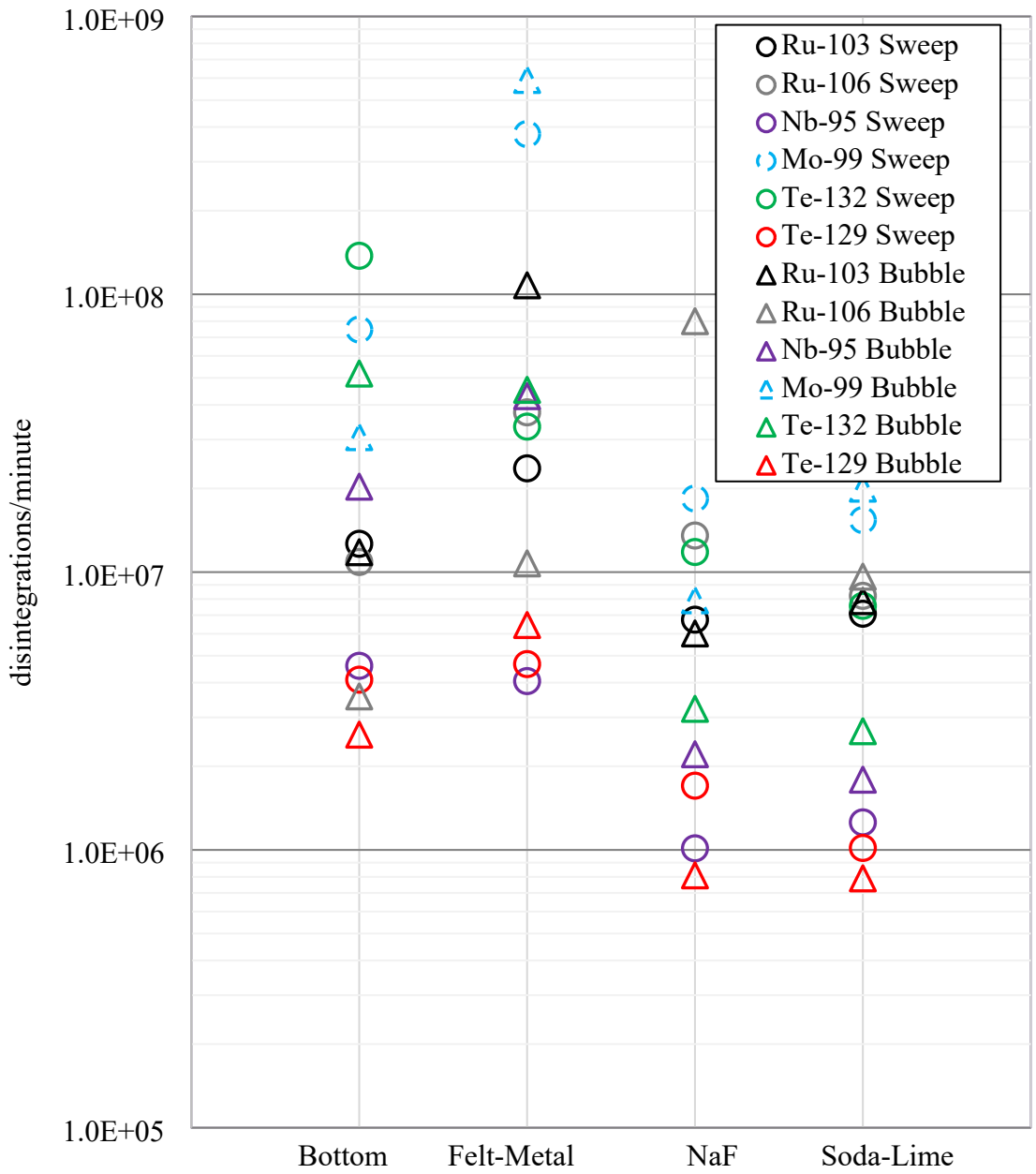

Fig. 10a. Plot of average tabulated data from reference [47, Table 10.5] of activity in four sections of the probe tube comparing bubbling-flow (given by triangles) and sweeping-flow (given by circles) collected aerosol. For this dataset, the sweeping-flow tests have comparable or sometimes more radioactivity deposited than the bubbling-flow tests. The data are shown in two plots (Figs. 10a and 10b) so that points can be distinguished.

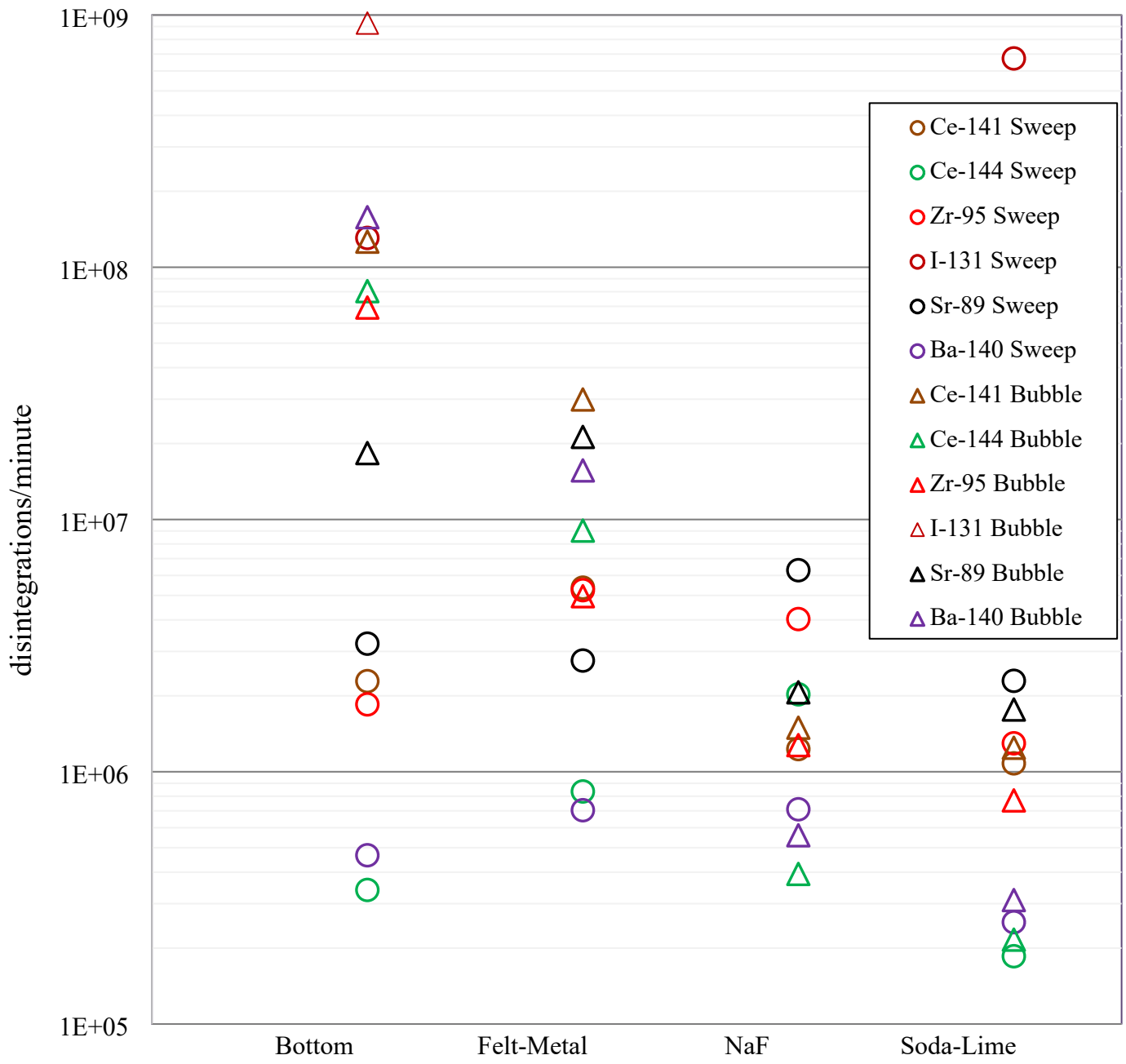

Fig. 10b. Plot of average tabulated data from reference [47, Table 10.5] of activity in four sections of the probe tube comparing bubbling-flow (given by triangles) and sweeping-flow (given by circles) collected aerosol. For this dataset, the sweeping-flow tests have comparable or sometimes more radioactivity deposited than the bubbling-flow tests. The data are shown in two plots (Figs. 10a and 10b) so that points can be distinguished.

Three possible mechanisms for releases of radioactive noble metals from quiescent molten salt given in reference [47, p. 107] are:

1. "recoils from beta emissions near the surface of the molten salt may cause ejection of tiny particles of fuel salt and of noble metals into the adjacent gas phase."
2. "differences in thermodynamic contact potentials between metals, salt, and the gas phase would tend to eject metal particles from the salt phase into the gas phase."
3. "the bursting of very tiny gas bubbles, perhaps formed by radioactive decay, might cause aerosol formation."

Other possible mechanisms for this release are discussed in reference [49] such as:

4. "a nonwetted particle on the surface of liquid could, if small enough, be dislodged by the molecular movements causing Brownian motion."

To confirm that radioactivity resulted in aerosol releases, the experiments were repeated with six sweeping-flow and two bubbling-flow experiments, but with unirradiated salt as given in reference [48, p. 150] and the same flow conditions as used previously. "The salt used was very similar to the MSRE fuel salt, except that none of the U^{4+} (0.22% ^{235}U) had been reduced to U^{3+}." The collected solutions in each of the four probe sections were "analyzed for lithium by flame photometry and uranium by delayed-neutron counting or by the fluorometric method."[48] There was difficulty making the measurements for lithium and uranium because the mass collected was very low, so the solutions used to extract the deposits in the four sections of the outlet probe tube were concentrated by a factor of 10. No significant deposits in the outlet tube

above the blanks were detected. The conclusion was that these "control tests indicated that the molten salt must be radioactive to produce the salt aerosol."[48, p.151] This is a puzzling result, and the authors noted that "**The mechanisms by which the metallic and salt aerosols are formed remain an open question**."[48]

From the electron micrographs and the collected deposits that passed through a felt-metal filter for 4-μm diameter particles, radioactive salt releases respirable radionuclides under even quiescent conditions. An understanding of the release mechanisms to explain the data is essential. Therefore, to obtain quantitative values for the masses and particle sizes produced for a given set of conditions, we are modeling the mechanisms suggested in reference [47], and the possibility of experimental artifacts that resulted in measurements of radioactive aerosol releases. We are working to answer the "open question" that was left unanswered in reference [48].

III.C. Consideration of Possible Experimental Artifacts

Molten FLiBe has a dynamic viscosity about seven times that of water, and a surface tension more than twice that of water at room temperature.[10] Therefore, for the bubble-flow experiments, very large bubbles of helium may form before breaking the surface. In this case, the salt level will rise in the reactor and may then contact and contaminate the outlet probe tube. To assess this possibility, a CFD simulation of the bubbling-flow experiments was performed with the salt properties at 600 °C,[8] a helium flow rate of 12.5 cm^3/min at 20 °C, and the geometry given in Fig. 6. Helium heated to 600 °C has a velocity out of the inlet tube of 0.0325 m/s. The salt properties in the simulation are $\rho = 2270$ kg/m^3, $\mu_{salt} = 0.0099$ kg/m/s, and $\sigma = 0.188$ N/m.[8] The helium viscosity of $\mu_{He} = 4.07\times10^{-5}$ kg/m/s is an extrapolation from 800 K,[50]

and the helium density computed from the ideal gas law is 5.58×10^{-2} kg/m^3. The CFD calculations were made with ANSYS/Fluent® version 2020/R1 using the multi-phase flow method Volume of Fluid (VOF).

Below in Fig. 11 is a snapshot of the simulation at 0.655 seconds in the center plane. As shown, the greenish-yellow bubbles have already detached and have not formed a single large bubble that would raise the salt level close to the inlet of the outlet probe. Therefore, molten salt level rising due to bubbling is not a likely experimental artifact. Work is continuing on modeling the bursting of a salt bubble cap to determine the sizes and amount of aerosol particles that may be produced by such a process.

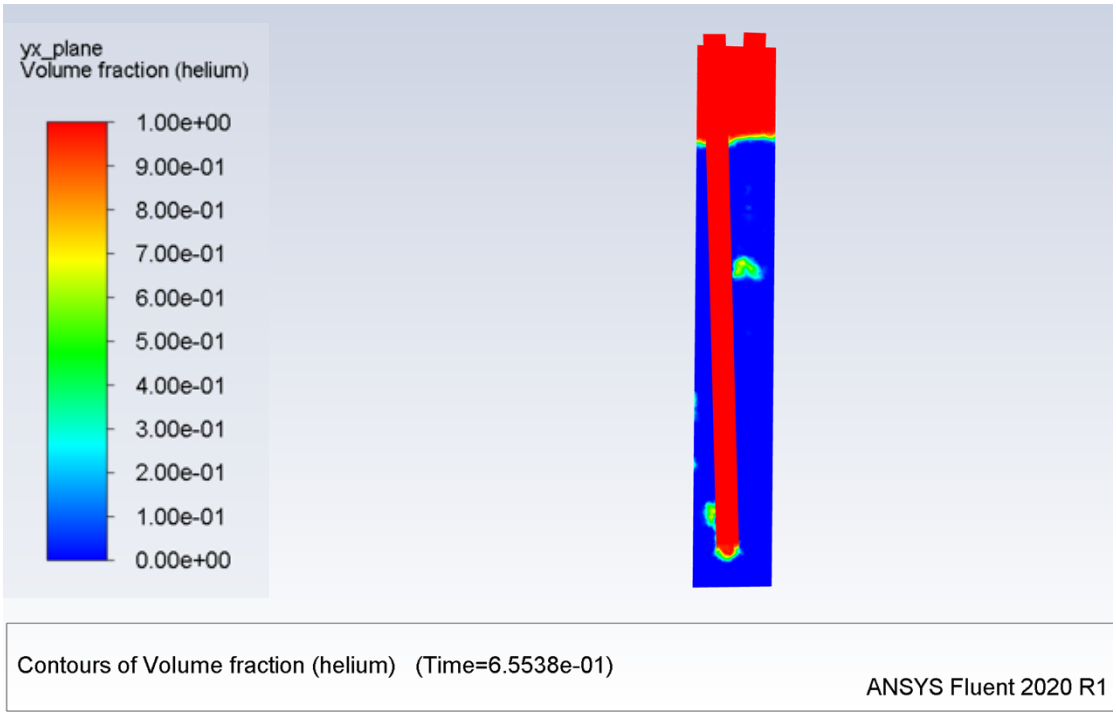

Fig. 11. CFD simulation of the bubbling-flow ORNL/MSRE experiments given on the right side of Fig. 7. The calculation shows that injected helium gas formed bubbles that were too small to contact the outlet probe tube or raise the salt level enough to contact the outlet probe tube if the tube was 6.35 mm (1/4 inch) above the salt.

Another possibility that could randomly affect aerosol collection is if the inlet tip of the outlet probe tube were sometimes contacted by the molten salt, and a liquid film of salt wetted the opening of the outlet probe tube. This can occur if the reported gap distance of ¼ inch (6.35 mm) were sometimes smaller. For example, the salt may have been a solid upon introduction into the reaction vessel, and the gap distance of ¼ inch (6.35 mm) was measured before heating the system to 600 °C. The inner diameter of the reaction vessel is estimated to be 17.3 mm. This may be a high estimate because according to reference [48, p. 145], the top of the reaction vessel inside diameter was increased to 5/8 inch (15.9 mm) after the first two series of tests. If 17.3 mm or 15.9 mm is used as the inside diameter, then the volume between the top of the salt to the bottom of the outlet tube for a ¼ inch (6.35 mm) height is 1.49 cm^3 or 1.26 cm^3, respectively. Using a recent compilation of salt data,[12] a correlation for the density of FLiBe including the solid range for temperatures in the range 555 K to 1200 K, where T is the temperature in degrees Kelvin is

$$\rho = 2.413 - (4.88\times10^{-4})T \quad g/cm^3 \ .$$

The actual initial salt temperature may have been lower than 555 K (282 °C). But to remain in the valid temperature range of the correlation, the volume change of FLiBe salt is calculated starting at 555 K (282 °C) to the temperature of the experiment 873 K (600 °C), and is given by,

$$\Delta V = Salt\_Mass\left(\frac{1}{\rho_{873}} - \frac{1}{\rho_{555}}\right) = 1.85 \text{ cm}^3.$$

Thus, the salt volume expansion is larger than the upper estimate of the volume between the salt and the outlet tube which is 1.49 cm^3. This implies that the salt may have expanded and contacted the outlet tube when heated to 600 °C for the original ¼ inch (6.35 mm) gap. There is also some thermal expansion of the reaction vessel and tubing, but that may not be enough to maintain the gap between the salt and outlet tube. If, as given in a later report,[48] the outlet tube were inserted to the upper range value of ½ inch (12.7 mm) from the salt surface, then the outlet tube would not contact the expanded salt. This analysis indicates the results are sensitive to the gap distance between the salt and outlet tube, and could affect both the sweeping-flow and bubbling-flow experiments. Since we cannot verify the distance between the salt and the outlet tube for the experiments, salt thermal expansion affecting the collection of fission products is an unverified possibility.

III.D. Aerosol Produced from the Film of a Bursting Bubble in an Aqueous Solution

We found no detailed reported measurements of molten salt bubble bursting, either bubbles of macroscopic size, or bubbles of microscopic size as suggested in reference [47, p. 107]. Instead, aerosol production has been reported for bursting bubble caps of aqueous solutions. The analysis and data from aqueous solution experiments are useful for understanding how and under what conditions we may expect aerosol generation from bursting bubbles of molten salt.

As discussed above, gas bubbles that rise in a liquid and rupture may form droplets by two main mechanisms, jet droplets from the inrush of liquid to fill the depression of the bubble, and film droplets from the thin bubble cap. Film droplets have the potential to form respirable

aerosol, so the remaining discussion is on this mechanism that may be one source for the observed MSRE respirable aerosol as given in Figure 8.

As noted in reference [43], many studies of bubbles inject gas from beneath the solution surface, and this gas rises to form a bubble at the surface that eventually ruptures. This would be representative of how bubbles may form in molten salt. However, to provide greater control on the size of the bubble, the bubble was formed by dipping the tip of a tube into a solution, and then lifting the tube.[43] A given volume of air was then pumped into the other end of the tube to obtain the desired bubble size. Then the tube was withdrawn, and the bubble remained floating on the liquid surface. With this method the bubble always ruptured starting at the top, whereas in other studies "bubbles preferentially rupture at points close to the meniscus that connects the bubble to the bulk."[43] Even though the bubble formation process is not like what may occur in a molten salt reactor accident, this is the only data we found that used modern aerosol instrumentation to measure the aerosol particle size distributions for each bubble, with varying solution properties and varying bubble size. In addition, this report also provides the measured film thickness just before the bubble burst. Some of the data[43] is given below in Fig. 12 for measurements made with a Condensation Particle Counter (CPC) and an Aerodynamic Particle Sizer (APS). The particles were dried before reaching the aerosol instruments and were therefore biased to smaller particle sizes. Because the upper size detection limit of the CPC is given as 1 micrometer, that would correspond to a wet 10 micrometer diameter droplet that had 99.9% of the particle volume vaporized by drying. Such a wet droplet would be originally respirable, and so would the dried droplet. Therefore, the CPC data may be used to determine the number of respirable particles produced from a single bursting bubble since aqueous droplets that are 10 micrometers in diameter and smaller are respirable.

From the left side of Fig. 12, the number of respirable particles from a single bubble is on the order of thousands and increases with increasing bubble diameter. From the right side of Fig. 12, the number of particles produced decreases with increasing surface tension. Water at ambient conditions has a surface tension of about 73 mN/m and there are high-speed photographs of very small droplets released by water bubble bursting.[51,52] However, in reference [43], a surfactant was added in the experiments to reduce the surface tension to 50 mN/m or less. Pure molten salts, such as FLiBe and FLiNaK, have surface tensions over 150 mN/m at 800 °C, and the surface tension of pure KCl-$MgCl_2$ is over 70 mN/m at 800 °C.[10] For the fluoride salts, if the data on the right side of Fig. 12 are extrapolated to a surface tension of 150 mN/m, bubble rupture may not result in respirable particle release. Extrapolating may not be valid and does not support the assumption that the data in Fig. 8 were due to bubble cap rupture. Another consideration is that the salt may be contaminated with particles of noble metals, abraded graphite, and/or corrosion products. Colloidal suspensions act as a surfactant that can lower the surface tension.[9,53] Other than for MSRE, we have not found data of the respirable aerosol produced from molten salt. Experiments are needed to resolve the discrepancy between the data in Fig. 8 and the extrapolation of the data on the right side of Fig. 12. Furthermore, as shown on the left side of Fig. 12, the bubble diameter is also important, and that needs to be determined as a function of the agitation level and contaminants in the salt.

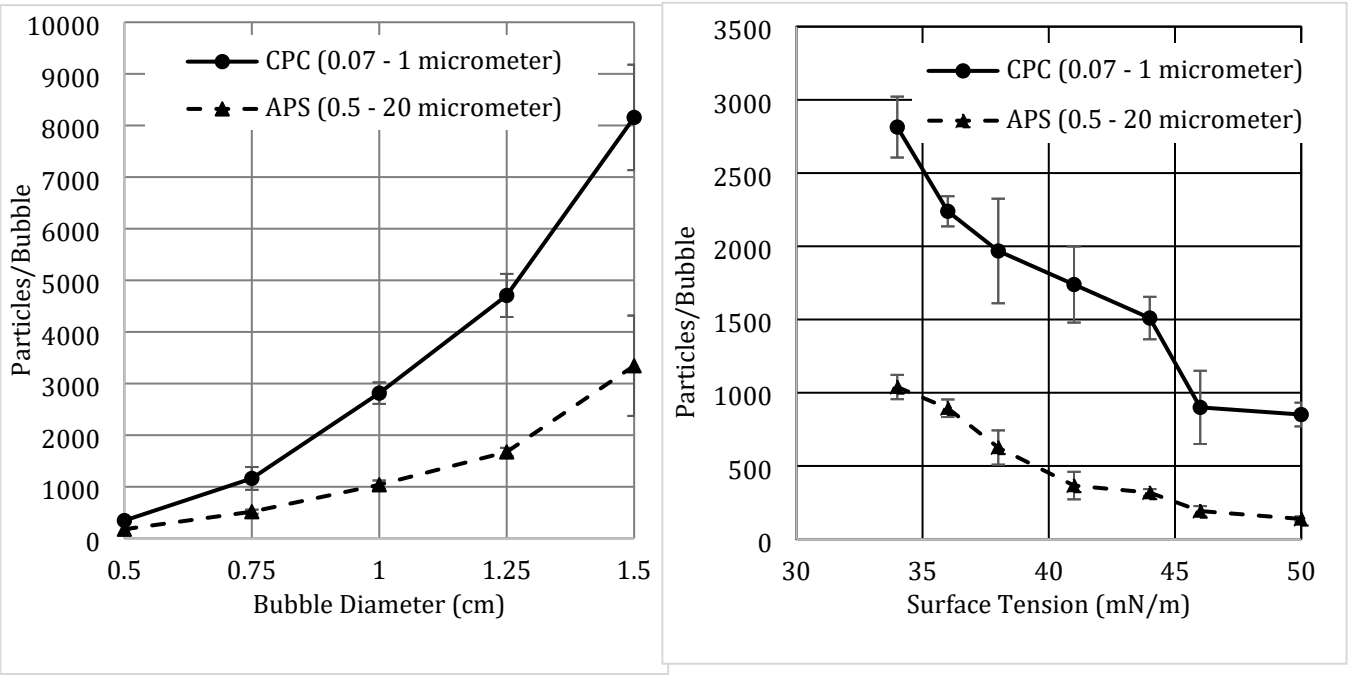

Fig. 12. Aerosol particles generated by a bursting bubble of an aqueous solution.[43]

IV. MELCOR INCORPORATION OF THE GRTR SUBMODEL

IV.A. Model Assumptions

A MELCOR molten salt control volume consists of a salt pool of uniform composition, temperature, and pressure, and may also include structures. The atmosphere above the salt, if present, includes non-condensible gases, aerosols, condensible vapors, and possibly structures. MELCOR includes models for heat and mass transfer, and vapor and aerosol processes for the atmosphere in a control volume. Condensible vapors, non-condensible gases, and aerosol particles released from or to the molten salt transfer mass between the atmosphere and the salt pool. Radionuclides that are deposited on structures in contact with the salt transfer heat to both the salt and structure via radioactive decay. In addition, the GRTR submodel allows for a top

layer of foaming salt with bubbles that contain insoluble fission products at a different concentration than in the bulk salt solution. Such a layer was observed in the MSRE.[8,54]

The mass transfer process of insoluble particles has been modeled for the MSRE.[9,54] Reference [54] states, "It is generally agreed that most of the fission products from niobium through tellurium are reduced to metals in the fuel salt, that they migrate to metal and graphite surfaces and to salt-gas interfaces, and that they adhere to the surfaces with varying degrees of tenacity." Determining the tenacity of the fission products onto surfaces in molten salt is a recognized research area.[55] For now, these particles are modeled as adhering to the metallic structures until data are available to indicate the level of disruption (i.e., either mechanical or thermal) needed to remove these particles. Therefore, the dashed arrow in Fig. 1 only points one way from Form 2 to deposits on heat structures. However, deposits may move between Form 2 and core surfaces which is shown as a double-headed dashed arrow.

In summary, radionuclides can be released from the salt as noble gases and by vaporization of volatile fission products. The vaporization process can result in respirable aerosol particles once the volatile species encounter a colder atmosphere, which will condense these vapors. There is evidence from MSRE that aerosol particles may also be released by agitation that engulfs gas and thereby forms bubbles. The cap of bubbles at the surface of a liquid has been shown to produce respirable aerosol particles for aqueous solutions with a surface tension less than 50 mN/m. The surface tension is much higher for pure salts being considered for an MSR, and therefore bubble bursting in molten salt may not produce respirable aerosol. Because respirable particles were observed at the MSRE, bubble bursting is therefore included in the GRTR submodel until data are available to exclude this phenomenon.

IV.B. Model Transport Equations

The transport to surfaces in contact with the salt and releases are calculated simultaneously but shown as two steps in Fig. 1 for clarity. Transport of mass and heat to and from surfaces makes the problem time dependent. Mass is also exchanged between the top surface of the pool and the atmosphere above the salt pool. Radioactive decay is included in the MELCOR calculations to provide heat and change in mass but is not given in the following equations. Volatile species and aerosol particles from the gas-liquid interface layer may be transported from the pool to the atmosphere above the pool. Aerosol deposition from the atmosphere to the pool provides a source term for the pool. If there are soluble species in the deposited aerosol, they will be dissolved in the next timestep when an equilibrium calculation is performed.

The conservation equations expressed in term of the masses and concentrations of species i in form j = 1, 2, 3, 4, 5 is given by $M_{i,j}$ and $C_{i,j}$, respectively. For simplifying these expressions, the core surfaces are included in the equations below, but deposits in the core are tracked separately in the code. The equations for $M_{i,j}$ are given next with the following notation,

A_{st} = salt top surface area,

A_{hs} = heat structure surface area in contact with the salt,

$C_{k,vap}$ = vapor concentration of species k in the atmosphere above the salt,

$H_{p\to q}$ = mass transfer coefficient of form p to form q,

$H_{p\to aer}$ = mass transfer coefficient of form p to aerosol by bubble bursting,

$H_{p\to vap}$ = mass transfer coefficient of form p to vapor in the atmosphere,

V = permanent gas release rate, and

t = time.

The values of $H_{p\to q}$ will depend on the geometry and flow conditions and are user input control functions based on correlations discussed in the next section.

Soluble mass in Form 1 changes due to vaporization and aerosol release and is given by,

$$\frac{d(M_{i,1})}{dt} = -A_{st}H_{1\to vap}(C_{k,1} - C_{k,vap}) - A_{st}H_{1\to aer}C_{i,1} \qquad (k = \text{volatile species only}). \quad (1)$$

The first term on the right is nonzero only for volatile species.

Insoluble mass in Form 2 changes due to deposition on structures and transport to the gas-liquid interface. This mass change is given by,

$$\frac{d(M_{i,2})}{dt} = -A_{hs}H_{2\to 4}(C_{i,2}) - A_{st}H_{2\to 3}(C_{i,2} - C_{i,3}) \qquad (i = \text{insoluble species only}). \qquad (2)$$

We assume that the deposit on structures is tenacious and remains attached to the structure, so there is no concentration difference in the first term on the right side of Eq. (2). However, the deposit on the core structures may be excluded at the users' discretion.

Mass in the gas-liquid interface can increase by aerosol deposition from the atmosphere, decrease by aerosol release, and increase by insoluble species transported to the interface. These three processes for only insoluble species i are given by,

$$\frac{d(M_{i,3})}{dt} = (Aerosol\ Deposition)_i - A_{st}H_{3\rightarrow aer}(C_{i,3}) + A_{st}H_{2\rightarrow 3}(C_{i,2} - C_{i,3}). \quad (3)$$

Insoluble mass adhering to structures in contact with the salt accumulates according to,

$$\frac{d(M_{i,4})}{dt} = A_{hs}H_{2\rightarrow 4}(C_{i,2}) \qquad (i = \text{insoluble species only}). \quad (4)$$

Any non-condensible gases, such as Xe and Kr in the molten salt are tracked separately as Form 5 in the GRTR submodel. A simple conservative model is to release all such gases above the solubility limit to the atmosphere, and neglect delays for the time the noncondensible gases need to reach the top of the pool. However, if the release rate is known or assumed, the rate of change of permanent gas mass in the pool is given by,

$$\frac{d(M_{i,5})}{dt} = (Source)_i - A_{st}V(C_{i,5}) \qquad (i = \text{permanent gas}). \quad (5)$$

If the solubility and time to release from the pool is neglected, then the mass of non-condensible gases in the pool is zero, and any noncondensible gas released into the pool at the beginning of a timestep is always released into the atmosphere at the end of the timestep. If there is no vapor space in the control volume, then the Form 5 gases remain in the molten salt.

IV.C. Model Parameters

The GRTR molten salt model developed for MELCOR as given by Eqs. (1-5) is very general and includes known and possible phenomena. This is intentional so that the user may investigate the relative importance of phenomena and decide what is worth further analysis or experimentation. A model with all the phenomena discussed in this work will include parameters that are unknown. Therefore, the code was written to allow users to specify model parameters in the input via user-defined control functions. This also enables the user to turn on and off selected phenomena in the model.

If an adequate database is not available for Thermochimica, then the GRTR submodel in MELCOR is designed to accept user-specified control functions or tables for the solubilities and vapor pressures. One may choose to use the color-coded periodic table as a guide for determining fission product solubility.[7] For vapor pressures of soluble fission products, the data for a specific salt is a useful guide.[20]

A potential process for direct aerosol release is for bubble cap bursting that may release particles with a composition the same as the salt pool and particles at the interface layer. The settling of aerosol particles into the pool is a source term for the third form and MELCOR provides the rate, composition, and sizes of aerosol particle settling.

All the mass transfer coefficients ($H_{p\rightarrow q}$, $H_{p\rightarrow aer}$, $H_{p\rightarrow vap}$) and areas (A_{st}, A_{hs}) can be provided as user input with user-defined control functions. For a well-mixed pool of molten salt, the mass transfer of a species to a surface can be modeled by analogy with heat transfer.[24,50] The correlations for heat transfer are applied for mass transfer with the Schmidt number replacing the Prandtl number, and the Sherwood number replacing the Nusselt number. This approach was used previously with MELCOR.[25] For the Sherwood number, the diffusivity of a species is

needed and can be estimated for fission products in the gas phase.[25] The diffusivity of a colloidal particle is given by[37]

$$\mathcal{D} = \frac{kT}{3\pi D\eta} \tag{6}$$

where k is Boltzmann's constant, T is the absolute temperature, D is the particle diameter, and η is the solution viscosity.

The observed respirable aerosol particles at the MSRE may be due to bubble bursting, or a radiological process.[48] The mass transfer coefficient $H_{p\rightarrow aer}$ is difficult to determine. Work is continuing to determine the number and sizes of aerosol particles for a range of accident conditions.

V. EXAMPLE PROBLEM

To demonstrate an application of MELCOR that uses the GRTR submodel, reference [56] has a simulation of a LOCA (Loss of Coolant Accident), with a 10% pipe break of the salt drain line in the Mark-1 Pebble-Bed Fluoride-Salt-Cooled High-Temperature Reactor (PB-FHR) Power Plant.[57] The details of the design and accident are given in references [57] and [56], respectively, and will not be repeated here. For the simulation, cesium released from the pebbles into the molten salt included subsequent mass transfer of Cs and CsF from the salt to the atmospheres of the control volumes. Thermochimica was called as needed within MELCOR for each time step and for each control volume over the 24 hours of simulation to determine the vapor pressure of the Cs and CsF, as given by Fig. 3 in this work. Due to limitation in the

available molten salt thermodynamic database, the pool chemistry and release calculations were limited to just the cesium behavior in the molten salt.

The results of the simulation are given in Fig. 13 with time on the x-axis starting at zero for the time cesium is released from the pebbles. The core outlet salt temperature is given on the right y-axis as a solid curve, and the fraction of the cesium inventory released from the pebble, in the liquid salt or vaporized from the liquid salt are given on the left y-axis as dashed, dotted, and dash-dotted curves, respectively. The cesium release fraction from the fuel builds up from approximately 10^{-8} at the start of the transient to 3.1×10^{-4} by 24 hours. Initially, all the cesium is retained in the molten salt. However, once the salt temperature exceeds 950 °C at about 7.3 hours, which is significantly above the expected operating temperature, the fraction vaporized increases to about 10^{-6} by 8.3 hours. As noted earlier, the solubility effect dramatically impedes vaporization, but is not an absolute barrier to fission product vaporization.

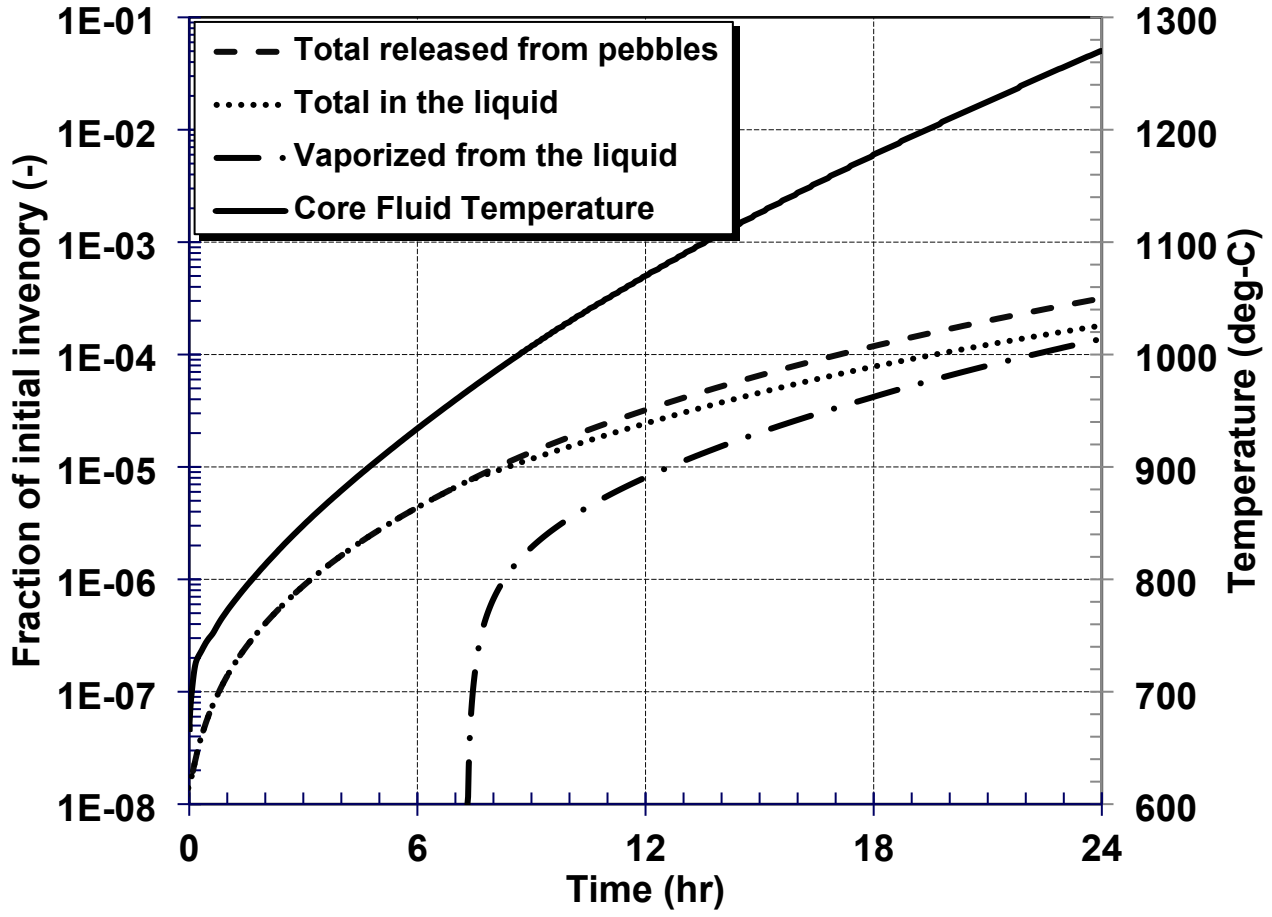

Fig. 13. Simulated cesium releases from a LOCA (10% pipe break of the salt drain line) in the Mark-1 Pebble-Bed Fluoride-Salt-Cooled High-Temperature Reactor (PB-FHR) Power Plant. Only the solid curve uses the right y-axis for the temperature, the three other curves use the left y-axis.

VI. SUMMARY AND RECOMMENDATIONS

The GRTR submodel has been incorporated into MELCOR. The model tracks the radionuclides released into the salt at the beginning of a timestep and calculates the masses of each radionuclide in five forms; (1) dissolved in the salt, (2) suspended in the salt as insoluble particles, (3) residing as insoluble particles at the gas-liquid interface, (4) particles adhering to structures in contact with the salt, and (5) gases released to the atmosphere above the pool. All the revised element masses in these five forms are passed back to MELCOR at the end of a GRTR timestep.

The tracking of radionuclides within GRTR is performed in three steps.

Step 1: Equilibrium

The GRTR submodel establishes the equilibrium conditions in the salt to determine the solubility and vapor pressure of each element in the simulation. This is accomplished using either the GEM code Thermochimica, which is now part of MELCOR, or through user input control functions. Based on this calculation, insoluble mass is placed into the colloid form, and soluble mass remains in the salt. Comparisons with experimental data for solubility and vapor pressure were given to demonstrate that the trends and fairly good agreement can be obtained with Thermochimica using the JRCMSD.

Future/Needed Work for Step 1: Equilibrium

The ability to determine vapor pressure and solubility by a GEM code for a specific element is currently constrained by the thermodynamic database. As noted previously in

the example problem, cesium was the only fission product of interest for which at the time the JRCMSD had data for fluoride salts. We would have preferred to include other fission products in the analysis had such data existed. Furthermore, the interaction of cesium with those fission products should be captured. Thus, a high priority need for this step is thermodynamic data for fission product elements, such as iodine and silver in salts at operational and severe accident temperatures. In addition, similar data are needed for fission product elements in the fifth row of the periodic table, especially those characterized as sometimes soluble, such as niobium, tellurium, cadmium, selenium, and zinc.

Step 2: Transport

Insoluble fission products are modeled as very small colloidal particles in the salt which is Form 2. These particles may be transported to the gas-liquid interface and thus are transported to Form 3. The colloidal particles may also deposit on heat structures or the core, and then are in Form 4.

Future/Needed Work for Step 2: Transport

The transport rates among Forms 2, 3, and 4 can be obtained from comparable heat and mass transfer correlations. Correlations existing in MELCOR can be used, or the user can supply control functions for this step. Data and analysis would be useful to determine the conditions for which deposited particles become resuspended. Similarly, data and analysis are needed for the buildup of particles at the gas-liquid interface as observed at the MSRE.

Step 3: Release

Determining radionuclide release to a cell atmosphere is an essential part of the GRTR submodel. The release may occur as vapor from Forms 1 or 5. Vapor transport rates to the atmosphere are available if the geometry, conditions, and vapor pressure are known. Subsequent vapor condensation to form aerosol particles in a cooler atmosphere is available in MELCOR. Aerosol particle releases from Form 3, or the salt pool in general, may occur naturally as reported for the MSRE separate effects experiments, or by an agitation process.

Future/Needed Work for Step 3: Release

As discussed in this work for the ORNL separate effects experiments, the mechanism(s) for respirable aerosol particle release from a quiescent radioactive molten salt pool is unknown. Resolving the mechanism is a high priority and essential for modeling the process for a range of accident conditions. For agitated liquids that splash and engulf gas, there has been much work for aqueous solutions. Data and analysis are needed for molten salts which have a significantly higher viscosity and surface tension than aqueous solutions. Such experiments need to be performed with radioactive and nonradioactive molten salts and a wide range of temperatures, including temperatures much above the normal operating temperature. To determine the particle sizes generated, modern aerosol instrumentation based on laser light scattering and aerodynamic particle sizing are needed to establish the mass and rate of aerosol release for a severe accident.

ACKNOWLEDGMENTS

We thank Richard Denning for informing the first author of a report[47] with data on aerosol particles collected in separate effects experiments in the MSRE. The ANSYS/Fluent® code was used to compute the CFD solutions and is a product of the ANSYS® Corporation. Assistance with ANSYS/Fluent® was provided by Daniel Chaparro, Tom Chadwick, and Sina Ghods of Phoenix Analysis and Design Technologies, PADT Inc. From Sandia National Laboratories we thank David Luxat for program management and John Reynolds for computer assistance. Most importantly we thank the U. S. Nuclear Regulatory Commission and the U. S. Department of Energy for funding different parts of this work.

Disclosure Statement

No potential conflict of interest was reported by the authors.

Funding

This article has been authored by an employee of National Technical & Engineering Solutions of Sandia, LLC under Contract No. DE-NA0003525 with the U. S. Department of Energy (DOE). The employee owns all right, title and interest in and to the article and is solely responsible for its contents. The United States Government retains and the publisher, by accepting the article for publication, acknowledges that the United Stated Government retains a non-exclusive, paid-up, irrevocable, world-wide license to publish or reproduce the published form of this article or allow others to do so, for United States Government purposes. The DOE will provide public

access to these results of federally sponsored research in accordance with the DOE Public Access Plan https://www.energy.gov/downloads/doe-public-access-plan.

The U. S. Nuclear Regulatory Commission funded the MELCOR work and the GRTR submodel development. The U. S. Department of Energy through the NEAMS program funded research on modeling aerosol production at the gas-liquid interface.

References

1. L. L. Humphries, B. A. Beeny, F. Gelbard, T. Haskin, D. L. Louie, R. C. Schmidt, and N. E. Bixler, "MELCOR Computer Code Manuals, Vol. 2: Reference Manual, Version 2.2.18019," SAND2021-0241 O, Sandia National Laboratories, Albuquerque, NM (2021).

2. L. L. Humphries, B. A. Beeny, F. Gelbard, D. L. Louie, J. Phillips, R. C. Schmidt, and N. E. Bixler, "MELCOR Computer Code Manuals, Vol. 1: Primer and Users' Guide, Version 2.2.18019," SAND2021-0726 O, Sandia National Laboratories, Albuquerque, NM (2021).

3. C. W. Forsberg, J. D. Stempien, M. J. Minck and R. G. Ballinger, "Understanding and Pathways to Avoid Major Fuel Failures and Radionuclide Release in Fluoride Salt-Cooled High-Temperature Reactor Severe Accidents," *Nuclear Technology,* **194**, 295-313 (2016); https://doi.org/10.13182/NT15-87.

4. C. F. Baes, "The Chemistry and Thermodynamics of Molten Salt Reactor Fuels," *Journal of Nuclear Materials*, **51**, pp. 149-162 (1974).

5. W. R. Grimes, "Molten Salt Reactor Chemistry," *Nuclear Applications Technology,* **8** (2) pp. 137-155 (1970).

6. J. D. Stempien, R. G. Ballinger and C. W. Forsberg, "Preliminary Fission Product Behavior in the Fluoride Salt-Cooled High-Temperature Reactor," *Transactions of the American Nuclear Society*, *Reactor Systems and Advanced Measurement Techniques,* **109**, pp. 625-628 (2013).

7. P. F. Britt, "2017 ORNL Molten Salt Reactor Workshop," ORNL Conference Center, Tennessee, October 3-4 (2017).

8. E. L. Compere, S. S. Kirslis, E. G. Bohlmann, F. F. Blankenship, and W. R. Grimes, "Fission Product Behavior in the Molten Salt Reactor Experiment," ORNL-4865, Oak Ridge National Laboratory, Oak Ridge, TN (1975).
9. S. A. Walker and W. Ji, "Species Transport Analysis of Noble Metal Fission Product Transport, Deposition, and Extraction in the Molten Salt Reactor Experiment," *Annals of Nuclear Energy,* **158**, 108250, August (2021); https://doi.org/10.1016/j.anucene.2021.108250.
10. M. S. Sohal, M. A. Ebner, P. Sabharwall, and P. Sharpe, "Engineering Database of Liquid Salt Thermophysical and Thermochemical Properties," INL/EXT-10-18297, March (2010), Idaho National Laboratory, Idaho Falls, ID (2010).
11. R. Serrano-Lopez, J. Fradera and S. Cuesta-Lopez, "Molten Salts Database for Energy Applications," *Chemical Engineering and Processing,* **73**, pp. 87-102 (2013); https://doi.org/10.1016/j.cep.2013.07.008.
12. R. R. Romatoski and L. W. Hu, "Fluoride salt coolant properties for nuclear reactor applications: A Review," *Annals of Nuclear Energy,* **109**, pp. 635-647 (2017); https://doi.org/10.1016/j.anucene.2017.05.036.
13. J. Jerden, "Molten Salt Thermophysical Properties Database Development: 2019 Update," ANL/CFCT-19/16, Argonne National Laboratory, Lemont, IL (2019); https://doi.org/10.2172/1559846.
14. J. Magnusson, M. Memmott, and T. Munro, "Review of Thermophysical Property Methods Applied to Fueled and Unfueled Molten Salts," *Annals of Nuclear Energy,* **146** 107608 (2020); https:/doi.org/10.1016/j.anucene.2020.107608.

15. M. H. A. Piro and T. M. Besmann, "Thermochimica User Manual v1.0," ORNL/TM-2012/576, Oak Ridge National Laboratory, Oak Ridge, TN (2012).
16. M. H. A. Piro and T. M. Besmann, "The Thermochemistry Library Thermochimica and its Application to Multi-Physics Simulations," TMS2013 Annual Meeting Supplemental Proceedings, TMS (The Minerals, Metals & Materials Society) (2013).
17. M. H. A. Piro, S. Simunovic, T. M. Besmann, B. J. Lewis, and W. T. Thompson, "The Thermochemistry Library Thermochimica," *Computational Materials Science,* **67**, pp. 266-272 (2013); https://doi.org/10.1016/j.commatsci.2012.09.011.
18. O. Beneš and R. J. M. Konings, "Chapter 4 – Thermodynamic Calculations of Molten-Salt Reactor Fuel Systems," in F. Lantelme and H. Groult (Eds.), Molten Salt Chemistry: From Lab to Applications, Elsevier, pp. 49-78 (2013).
19. O. Beneš and R. J. M. Konings, "5.18 – Molten Salt Reactor Fuel and Coolant," Comprehensive Nuclear Materials (Second Edition) **5**, 609-644 (2020); https://doi.org/10.1016/B978-0-12-803581-8.11790-4.
20. E. Capelli, O. Beneš, and R. J. M. Konings, "Thermodynamics of soluble fission products cesium and iodine in the molten salt reactor," *Journal of Nuclear Materials*, **501**, 238-252 (2018); https://doi.org/10.1016/j.nucmat.2018.01.024.
21. A. D. Pelton, P. Chartrand, and G. Eriksson, "The modified quasi-chemical model: Part IV. Two-sublattice quadruplet approximation," *Metallurgical and Materials Transactions A*, 32 (6), 1409–1416 (2001); https://doi.org/10.1007/s11661-001-0230-7.
22. G. Lambotte and P. Chartrand, "Thermodynamic optimization of the (Na_2O+SiO_2+NaF+SiF_4) reciprocal system using the Modified Quasichemical Model in

the Quadruplet Approximation", *The Journal of Chemical Thermodynamics*, **43** (11), 1678–1699 (2011); https://doi.org/10.1016/j.jct.2011.05.038.

23. M. Poschmann, P. Bajpai, B. W. N. Fitzpatrick, and M. H. A. Piro, "Recent developments for molten salt systems in Thermochimica", *CALPHAD: Computer Coupling of Phase Diagrams and Thermochemistry*, 75 (September), 102341 (2021); https://doi.org/10.1016/j.calphad.2021.102341.
24. R. B. Bird, W. E. Stewart, and E. N. Lightfoot, *Transport Phenomena, Revised Second Edition,* Wiley (2007).
25. J. Kalilainen, S. Nichenko, and J. Krepel, "Evaporation of Materials from the Molten Salt Reactor Fuel Under Elevated Temperatures," *Journal of Nuclear Materials,* **533**, 152134 (2020); https://doi.org/10.1016/j.jnucmat.2020.152134.
26. N. Bixler, F. Walton, J. Leute, L. Eubanks, R. Haaker, and K. McFadden, "MACCS (MELCOR Accident Consequence Code System) User Guide," SAND2021-1588, Sandia National Laboratories, Albuquerque, NM (2021).
27. D. R. Olander, G. T. Fukuda, and C. F. Baes, "Equilibrium Pressures over BeF_2/LiF (FLIBE) Molten Mixtures," *Fusion Science and Technology* **41**, pp. 141-150 (2002).
28. J. Zhang, C. W. Forsberg, M. F. Simpson, S. Guo, S. T. Lam, R. O. Scarlat, F. Carotti, K. J. Chan, P. Singh, W. Doniger, K. Sridharan, and J. R. Keiser, "Redox potential control in molten salt systems for corrosion mitigation," *Corrosion Science,* **144**, pp. 44-53 (2018); https://doi.org/10.1016/j.corsci.2018.08.035.
29. C. J. Barton, W. R. Grimes, and R. A. Strehlow, "Solubility and Stability of PuF_3 in Fused Alkali Fluoride-Beryllium Fluoride Mixture," ORNL-2530, Oak Ridge National Laboratory, Oak Ridge, TN (1958).

30. C. J. Barton, "Solubility of Plutonium Trifluoride in Fused-Alkali Fluoride-Beryllium Fluoride Mixtures," *Journal of Physical Chemistry,* **64**, 306-309 (1960).

31. C. J. Barton, M. A. Bredig, L. O. Gilpatrick, and J. A. Fredrisksen, "Solubility of Cerium Trifluoride in Molten Mixtures of Lithium, Beryllium, and Thorium Fluorides," *Inorganic Chemistry,* **9** (2), 307-311 (1970).

32. J. C. Mailen, F. J. Smith, and L. M. Ferris, "Solubility of PuF_3 in Molten 2LiF-BeF_2," *Journal of Chemical and Engineering Data,* **16** (1) 68-69 (1971).

33. A. A. Lizin, S. V. Tomilin, V. V. Ignat'ev, A. G. Osipenko, M. V. Kormilitsyn, and N. Yu. Nezgovorov, "Joint Solubility of PuF_3 and CeF_3 in Ternary Melts of Lithium, Thorium, and Uranium Fluorides," *Radiochemistry,* **57 (**1) pp. 36–42 (2015); https://doi.org/10.1134/S1066362215010063.

34. A. A. Lizin, S. V. Tomilin, A. G. Osipenko, N. Yu. Nezgovorov, V. V. Ignat'ev, and M. V. Kormilitsyn, "Investigation of PuF_3 and AmF_3 Solubility in 73LiF-27BeF_2 Melt," *Atomic Energy,* **126** (6) 368-371, October (2019); https://doi.org/10.1007/s10512-019-00566-6.

35. P. A. Demkowicz, J. D. Hunn, D. A. Petti, and R. N. Morris, "Key Results from Irradiation and post-irradiation examination of AGR-1 UCO TRISO Fuel," *Nuclear Engineering and Design,* **329,** 102-109 (2018); http://doi.org/10.1016/j.nucengdes.2017.09.005.

36. O. Beneš, E. Capelli, N. Vozarova, J. Y. Colle, A. Tosolin, T. Wiss, B. Cremer, and R. J. M. Konings, "Cesium and iodine release from fluoride-based molten salt reactor fuel," *Physical Chemistry Chemical Physics,* **23**, 9512 (2021); https://doi.org/10.1039/d0cp05794k.

37. R. J. Hunter, *Foundations of Colloid Science,* Volume I, Oxford Science Publications, p. 57 (1991).

38. F. J. Smith, L. M. Ferris, and C. T. Thompson, "Liquid-Vapor Equilibria in LiF-BeF_2 and LiF-BeF_2-ThF_4 Systems," ORNL-4415, Oak Ridge National Laboratory, Oak Ridge, TN (1969).

39. DOE Handbook, *Airborne Release Fractions/Rates and Respirable Fractions for Nonreactor Nuclear Facilities*, Volume 1, DOE-HDBK-3010-94, Reaffirmed (2013).

40. D. C. Blanchard and L. D. Syzdek, "Film Drop Production as a Function of Bubble Size," *Journal of Geophysical Research,* **93** (C4) 3649-3654 (1988); Paper Number 8C0013.

41. T. Ginsberg, "Aerosol Generation by Liquid Breakup from Sparging of Molten Pools of Corium by Gases Released During Core/Concrete Interactions," *Nuclear Science and Engineering,* **89** (1) 36-48 (1985).

42. F. Resch and G. Afeti, "Submicron Film Drop Production by Bubbles in Seawater," *Geophysical Research,* **97** (C3) 3679-3683 (1992).

43. W. R. Ke, Y. M. Kuo, C. W. Lin, S. H. Huang, and C. C. Chen, "Characterization of aerosol emissions from single bubble bursting," *Journal of Aerosol Science,* **109**, 1-12 (2017); https://doi.org/10.1016/j.jaerosci.2017.03.006.

44. D. C. Blanchard and L. D. Syzdek, "Water-to-Air Transfer and Enrichment of Bacteria from Bursting Bubbles," *Applied and Environmental Microbiology*, **43** (5) 1001-1005 (1982).

45. H. W. Kohn, "Bubbles, Drops, and Entrainment in Molten Salt," ORNL-TM-2373, Oak Ridge National Laboratory, Oak Ridge, TN (1968).

46. J. R. Engel, P. N. Haubenreich, and A. Houtzeel, "Spray, Mist, Bubble, and Foam in the Molten Salt Reactor Experiment," ORNL-TM-3027, Oak Ridge National Laboratory, Oak Ridge, TN (1970).

47. S. S. Kirslis and F. F. Blankenship "Fission Product Behavior," in M. W. Rosenthal, R. B. Briggs, and P. R. Kasten, "Molten-Salt Reactor Program Semiannual Progress Report: For Period Ending February 29, 1968," ORNL-4254, pp. 107-114, Oak Ridge National Laboratory, Oak Ridge, TN (1968).

48. S. S. Kirslis and F. F. Blankenship, "Fission Product Volatilization Tests," in Rosenthal, M. W. (Director) "Molten Salt Reactor Program, Semiannual Progress Report for Period Ending February 28, 1969," ORNL-4396, Oak Ridge National Laboratory, Oak Ridge, TN (1969).

49. F. F. Blankenship, "A Possible Origin of Smokes and Mists Emitted by MSRE Fuel," in "Molten-Salt Reactor Program Semiannual Progress Report for Period Ending August 31, 1970," ORNL-4622, pp. 70-71, Oak Ridge National Laboratory, Oak Ridge, TN (1971).

50. J. P. Holman, *Heat Transfer*, 5th edition, McGraw-Hill (1981).

51. H. Lhuissier and E. Villermaux, "Bursting Bubbles," *Physics of Fluids* **21**, 091111, (2009); https://doi.org/10.1063/1.3200933.

52. H. Lhuissier, and E. Villermaux, "Bursting Bubble Aerosols," *Journal of Fluid Mechanics*, **696**, pp. 5-44 (2012); https://doi.org/10.1017/jfm.2011.418.

53. Y. Hadidimasouleh and R. Riahifar, "Modeling of the Surface Tension of Colloidal Suspensions," *Surface Review and Letter,* **24** (4) 1750050 (2017); https://doi.org/10.1142/S0218625X17500500.

54. R. J. Kedl, “The Migration of a Class of Fission Products (Noble Metals) in the Molten-Salt Reactor Experiments,” ORNL-TM-3884, Oak Ridge National Laboratory, Oak Ridge, TN (1972).
55. R. S. Tanaka, “Quantified the Adhesion of Noble Metal Foulants on Structural Materials in a Molten Salt Reactor,” Massachusetts Institute of Technology, M.S. Thesis, Cambridge, MA (2017).
56. K. Wagner et al., “MELCOR Accident Progression and Source Term Demonstration Calculations for a FHR,” SAND2022-2751, Sandia National Laboratories, Albuquerque, NM (2022).
57. C. Andreades et al., “Technical Description of the “Mark 1” Pebble-Bed Fluoride Salt-Cooled High-Temperature Reactor (PB-FHR) Power Plant,” UCBTH-14-002, Department of Nuclear Engineering, University of California, Berkeley, (2014).